

# Mechanical reverse engineering approach for precise measurements of reproducing disc CAM

Mohammad S. Alsoufi <sup>1\*</sup>, Mohammed W. Alhazmi <sup>1</sup>, Sufyan Azam <sup>1</sup>

<sup>1</sup> Department of Mechanical Engineering, College of Engineering and Islamic Architecture, Umm Al-Qura University, Makkah, KSA

\*Corresponding author E-mail: [mssoufi@uqu.edu.sa](mailto:mssoufi@uqu.edu.sa)

## Abstract

This research paper focuses on reverse engineering in a mechanical engineering design domain. The paper presents the process of reversed disc CAM from an existing one and also the strategy for scanning and converting the scanned data using coordinate measuring machine (CMM) technology in the form of point cloud data into a 3D model of the disc CAM and finally measurement assessments. The copy of the existing part is in order to produce the original (existing) product design intent. This paper investigates the current aluminum, hardened steel and stainless steel disc CAM and the reversed disc CAM (including aluminum, hardened steel, stainless steel, PLA+, PLA, ABS+ and photo-polymer resin) in terms of the height variation, dimensional accuracy, surface roughness and skewness and kurtosis performance. These are done with the help of various instruments used for data acquisition and different software's used for data processing and modeling. These parameters of assessments have huge influences on the functional behaviour as well as the customers' quality perception of the products.

**Keywords:** Reverse Engineering; Geometric; Additive Manufacturing; CNC Machine; CMM.

## 1. Introduction

In today's intensely competitive worldwide market, reverse engineering (RE) and shape reconstruction (SR) plays an essential role in design domain and manufacturing through the increased use of shape acquisition and processing technologies in the new product development process and also in terms of reducing times for new product developments that meet all client expectations [1]. The application of shape theories to geometric modeling and variability characterization are paving the way to shape engineering and more generic methods for reverse engineering. Beyond a doubt, RE is recognized as a vital issue in the product design process which highlights inverse ways, deduction and discovery in design domain [2], and the RE procedure can be characterized by the flowchart shown in Figure 1.

The original definition (or terminology) of RE was made in hardware research. As time goes by, it has been defined by various expressions according to its applications in various fields [3]. Initially, RE was described as "the process of developing a set of specifications for a complex hardware system by an orderly examination of specimens of that system" [4]. RE is also defined as "the process of obtaining a geometric CAD model from 3D points acquired by scanning/digitizing current parts/products. The process of digitally capturing the physical entities of a component referred to as reverse engineering (RE), is often defined by researchers concerning their specific task" [5]. RE is also defined as "the process of analyzing a subject system to identify the systems components and their relationships and to create representations of the system in another form or at a higher level of abstraction" [6]. On the other hand, in the mechanical design domain, RE is defined as "the process that initiates the redesign process wherein a product is predicted, observed, disassembled, analyzed, tested, experienced and documented regarding its func-

tionality from physical principles, manufacturability and assemblability [7]. RE in the mechanical design domain has been considered as a method of understanding how a product works and the process of duplicating an object in order to obtain a surrogate 3D solid model or a clone, enhance its performance and to capture and apply the embedded knowledge to new mechanical design [8]. Although different expressions are used for RE, the meanings are fundamentally similar, and the ultimate goals are to acquire a better or new mechanical design from the existing one. Although RE theories and methods, traced back to the 1980s, were predominant in the area of software, hardware and biological systems, nowadays, RE techniques are applied in different areas, ranging from mechanical engineering to dentistry and medicine [9-12]. RE is now widely used in numerous applications, such as manufacturing, industrial design, and jewelry design and reproduction.

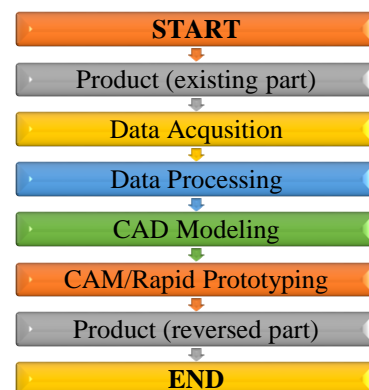


Fig. 1: Basic Phases of RE, Adapted from [13], [14].

## 1.1. Research purpose

RE plays a crucial role and has particular excellences respectively from the concept design to product manufacturing. The purpose and scope of this research paper is to make use of the reverse engineering (RE) technique as described as follows:

- Using the coordinate measuring machine (CMM) technology to acquire the cloud of point data of the original (existing) disc CAM of aluminum, hardened steel and stainless steel.
- Using a design software to construct the 3D solid model on the point and curve data creating the CMM.
- Discussing and modifying design parameters on the physical model created from the rapid prototyping (RP) technique and computer numerical control (CNC) machine.
- Combining RE technology by using a different method including an RP and CNC machine to the short development process, time and cost.
- Using different conventional and non-conventional technologies to assess the performance of RE including height variation, dimensional accuracy, surface roughness, skewness

and kurtosis of the original (existing) and reversed disc CAM.

- Using OriginLab 2018 software for analyzing the obtained data.

## 2. Material and methods

### 2.1. Material used for RE

Here, different engineering materials have been used in this study for reversed disc CAM including aluminum, hardened steel, stainless steel, PLA+, PLA, ABS+ and formlabs black V1 resin (photo-polymer). Bear in mind that aluminum, hardened steel and stainless steel of an original (existing) and reversed disc CAM comes from the same classified engineering material. Table 1 shows the summary of the machines used for original (existing) and reversed disc CAM including the weight and manufacturing time spend for completion. Besides, it shows that the average manufacturing time spends on completing one sample was between 1 to 2 hours with 100% density infill.

**Table 1:** Machine Used for Original (Existing) and Reversed Disc CAM Including the Weight and Manufacturing Time

Machine used	Status	Materials Stl. File	Materials used for RE	Materials Colour	Weight (g)	Manufacturing Time	
CNC Machine	Original Disc CAM	Aluminum	Aluminum	Light Metallic	44.6878	02hr:00m:00s	
		Hardened Steel	Harden Steel	Dark Metallic	123.7164	02hr:30m:00s	
		Stainless Steel	Stainless Steel	Dark Metallic	125.8712		
CNC Machine		Aluminum	Aluminum	Light Metallic	48.6886	02hr:00m:00s	
		Hardened Steel	Harden Steel	Dark Metallic	135.5268	02hr:30m:00s	
		Stainless Steel	Stainless Steel	Dark Metallic	137.6898		
		Aluminum			9.4053		
FDM 3D Printer	Reversed Disc CAM	Hardened Steel	PLA+	Grey	9.7221	05hr:59m:11s	
FDM 3D Printer		Stainless Steel				9.6950	
		Aluminum				7.2121	
FDM 3D Printer		Hardened Steel	PLA	Glass Blue	7.4304	05hr:59m:11s	
		Stainless Steel			7.5766		
FDM 3D Printer		Aluminum			4.8176		
		Hardened Steel	ABS+	White	5.0058	05hr:59m:11s	
SLA 3D Printer		Stainless Steel			4.9566		
		Aluminum			19.2947		
		Hardened Steel	Photo-polymer	Black	19.6597	03hr:32m:00s	
		Stainless Steel	Formlabs Black V1 Resin		19.5926		

### 2.2. Machine used for RE

In the present study, RE technology was used to make the 3D solid model of the disc CAM as it was difficult to make a 3D solid model in the absence of the original (existing) design as insufficient documentation supported this and, no plans nor drawings are available or correct. Besides, the provider has disappeared and did not manufacture the component anymore. So, RE is vital to be used in this research paper. Three different machines were used for reversed disc CAM namely computer numerical control (CNC) machine, fused deposition modeling (FDM) 3D printer and stereolithography (SLA) 3D printer.

#### 2.2.1. CNC machine

The CNC machine (purchased from Victor Taichung Machinery Works Co., Ltd.) was used in this investigation for reversing three different original (existing) disc CAMs including aluminum, hardened steel and stainless steel, which was initially generated from an STL file using a conventional contact-type CMM machine. A flat 8 mm end mill was used for machining the reversed disc CAM profile with a maximum spindle speed of 1909 rpm and a feed rate of 381.8 mm/min. The disc CAM was designed by using MSC ADAMS software V2014 machinery module with a maximum follower displacement of 40 mm. The 3D CAD model (.STEP) was then transferred into MASTERCAM X7 to generate an NC code for CNC machining. The NC code generated by the MASTERCAM X7 was then copied to the CNC machine interface software having a FANUC CNC controller.

#### 2.2.2. FDM 3D printer

The rapid prototyping (RP) is a stimulating new technology for users on account of the fact that it quickly creates 3D physical models and functional prototypes directly from computer-aided design (CAD) models [15]. The rapid tooling (RT) generally concerns the fast production of tooling using inserts. RP and RT are meant to compress time-to-market of products and, as such, are competitiveness-enhancing technologies in the global foundry industry [14]. Here, the personal FDM 3D printer (affordable do-it-yourself kits) used in this investigation was based on an open source digital model known as 'The BEAST', (available from Cultivate3D, Australia). This is a fully customized personal 3D printer which allows lightweight, low-cost, and very rapid prototyping compared to conventional machining (as with, for example, a CNC machine).

Here, CATIA® V5 R20 as multi-platform software is used for 3D modeling design and is also suited to computer-aided design (CAD). The 3D digital model design is then converted to an STL file using CATIA® V5 R20 itself. The STL is a file format native to the STL CAD software created by the 3D model system. Many other software packages support this file format; it is widely used for RP and CAD model. The KISSlicer PRO software assists the end-user in adjusting the build parameters and generates path information, and a G-code (geometric code) is subsequently generated which controls the extrusion head of the personal FDM 3D printer. Each RP device possesses proprietary strategies for the conversion of the design to a personal FDM 3D printable format.

Two related manufacturing processes were used including RE/CNC process (same engineering materials and manufacturing process) and RE/RP process (different engineering materials and manufacturing process). Table 2 shows a summary of the process parameters used in the personal FDM 3D printer. Bear in mind that the personal FDM 3D printer process parameters were identified from a previous study reported in [16-20]

**Table 2:** Process Parameter Selection of the FDM 3D Printer

Parameters	Values
Filament Material	PLA, PLA+, ABS+
AM Process	FDM (Fused Deposition Modeling)
Layer Height (mm)	0.1
Infill Density (%)	100
Nozzle Diameter (mm)	0.3
Nozzle Temperature (°C)	220
Printing Speed (mm/s)	32
Speed for non-print moves (mm)	72
Horizontal Shells (top and bottom layer)	3
Vertical Shells	3
Cooling Rate	built-in
Bed Temperature (°C)	Room Temperature
Room Temperature (°C)	25±1
Relative Humidity (% RH)	40±5
external perimeters extrusion width (layer width) (mm)	0.25
perimeters extrusion width (mm)	0.25
infill extrusion width (mm)	0.73
solid infill extrusion width (mm)	0.51
top infill extrusion width (mm)	0.25

### 2.2.3. SLA 3D printer

Here, the personal SLA 3D printer (affordable do-it-yourself kits) used in this investigation was based on an open source digital model (available from Formlabs, USA). This is a fully customized personal 3D printer which allows lightweight, low-cost, and very rapid prototyping compared to conventional machining (as with, for example, a CNC machine). In stereolithography (SLA) 3D printing, substantial parts are made by curing a liquid material, layer by layer, with a UV light source. The material used in such printing is called photopolymer. The FORMLABS 1 upside-down (inverted) SLA 3D printer was used to make the new and reversed disc CAM samples. The thermoplastic material used was black photopolymer resin V1 (FLGPBK01). The generated STL model was converted to 100 layers with a minimum layer thickness of 0.1 mm using the occupied software from FORMLABS itself. All the reversed samples were printed on a flat base having no supports. The generated samples were then washed in acetone for approximately 10 to 15 minutes. Finally, all the reversed samples were dried using an air blower and lifted in a comfortable ambient room temperature, generally taken as about 20°C.

Figure 2 shows a photograph of the original (existing) disc CAM including aluminum, hardened steel and stainless steel and reversed materials including aluminum, hardened steel, stainless steel, PLA+, PLA, ABS+ and formlabs black V1 resin (photo-polymer).

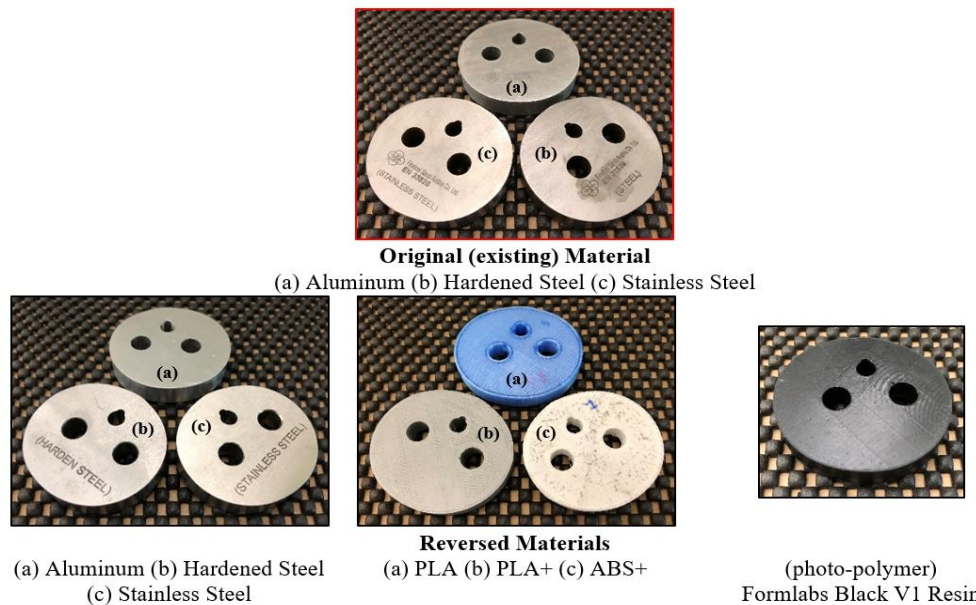


**Fig. 2:** Photograph of Original (Existing) Disc CAM Including Aluminum, Hardened Steel and Stainless Steel and Reversed Materials Including Aluminum, Hardened Steel, Stainless Steel, PLA+, PLA, ABS+ and Formlabs Black V1 Resin (Photo-Polymer).

### 2.3. Procedure and testing equipment

Three different test-rigs were used during this investigation including CMM, surface roughness and a digital Vernier caliper. Each device was used for a specific assessment. Figure 3 shows the techniques used for measuring the height variation of the original (existing) and reversed disc CAM at 0° (A), 45° (B), 90° (C), 135° (D), 180° E, 220° (F), 270° (G), 315° (H) and the middle. Also, it shows the techniques used for measuring the dimensional accuracy of the original (existing) and reversed disc CAM where (CG) indicates the vertical axis, (AE) indicates the horizontal axis and (BF and DH) indicates the diagonal axis. Finally, the conventional contact-type surface roughness test-rig was used to measure the average surface roughness,  $R_a$ , skewness,  $R_{sk}$ , and kurtosis,  $R_{ku}$  over the original (existing) and reversed disc

CAM profile at each angle of 0° (A), 45° (B), 90° (C), 135° (D), 180° E, 225° (F), 270° (G) and 315° (H).

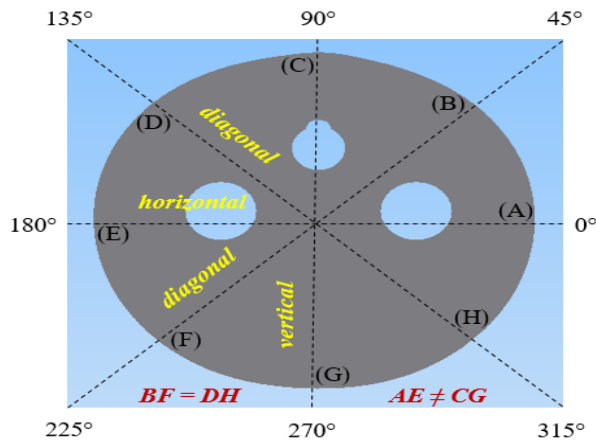


Fig. 3: Disc CAM Testing Procedure.

## 2.4. Coordinate measuring machine (CMM)

In this research work, RE is used to gather scientific knowledge about the disc CAM by physically examining it with the full support of conventional contact-type CMM for producing clouds of points, which define the surface geometry, as shown in Figure 4. CMM is an advanced and very precise machine used for dimensional data acquisition with direct contact probe and operated by direct computer control and equipped with various style. The disc CAM was scanned by using Eley Metrology's SP600 scanning probe (purchased from Eley Meteorology CMM Millennium, USA). The closed-loop scanning method was used with a point pitch of 0.5 mm. The scanning was carried out by the probe (Touch Trigger TP2/TP20) with the static head (PH6/PH6M). The diameter of the probe was 2 mm. Here, contact probe scanning devices are based on CMM technology, with +0.01 to 0.02 mm total range of the tolerance. However, depending on the size of the sample scanned, contact-type methods can be slow as each point cloud is generated sequentially at the tip of the probe. The CMM contact-type probe collects data by probes touching the disc CAM surface along the complete profile of that object. It gives the data in the form of point cloud which is then exported to CAD modeling software in order to convert it into a 3D CAD model. The CATIA® V5 R20 software is used for converting the point cloud data into the 3D CAD model. In this software, all the points are joined, Then, they are added to form the 3D model of the disc CAM. This 3D CAD model can be sued for preparation of the inspection program.



Fig. 4: Contact-Type CMM Engaged with Disc CAM.

## 2.5. Surface roughness profile measurements

In this research paper, the contact surface profile of all original (existing) and reversed disc CAMs was quantitatively analyzed in

order to determine the average surface roughness,  $R_a$ , skewness,  $R_{sk}$ , and kurtosis,  $R_{ku}$ , by using a conventional contact-type Taly-surf® profilometer (from Taylor Hobson, Inc. delivers 0.8 nm resolution over 12.5 mm measuring range, including 0.125  $\mu\text{m}$  horizontal data spacing, a nominal 2.0  $\mu\text{m}$  stylus was used with a normal load of 0.7 mN and selectable traverse speed down to 5  $\text{mm s}^{-1}$ . The traces were auto-leveled to a linear least-squares straight line and then filtered with a standard 0.8 mm cut-off wavelength.

Every test condition was repeated at least three times very carefully at different “new” locations on all original (existing) and reversed disc CAMs profile to ensure the repeatability and reproducibility of the obtained results. The new location was at least  $\pm 100 \mu\text{m}$  from the previous one. This approach should avoid any alteration of the counter-body surface profile, e.g., due to wear condition, which might occur during the test and affect the measurements in the following tests. All experiments were performed with a typical “ball-on-flat” arrangement applying a linear sliding contact at constant velocity over a specific distance. Assessments were performed by using single scan mode (forwards motion). Profiler at scan length of 10 mm, which is close to the size of the human fingertip [21-30].

The surface process parameters were selected according to the recommendations in the literature and also under consideration of the data processing facilities available [31-35]. The obtained data were reviewed and analyzed qualitatively with OriginLab® 2018 software. The measurement and resultant assessment of the desired disc CAMs were successfully carried out according to international standards. The high precision, repeatability and reproducibility of this technology make it appropriate for reverse engineering (RE) and roughness measurement.

## 3. Results and discussion

After scanning the original (existing) three disc CAM using a CMM machine to acquire the point cloud data for each disc CAM as shown in Figure 5 from the reverse engineering operation, the original (existing) disc CAM (including aluminium, hardened steel and stainless steel) and reversed engineering disc CAM (including aluminium, hardened steel, stainless steel, PLA+, PLA, ABS+ and photo-polymer resin) was measured precisely regarding the height variation, dimensional accuracy, surface roughness,  $R_a$ , skewness,  $R_{sk}$ , and kurtosis,  $R_{ku}$ . Bear in mind that all the points that were obtained from CMM as a point of cloud data were joined for the preparation of the 3D CAD model. The original (existing) STL data is scattered and contains some noise around the boundary of the model. This noise creates a problem while generating a solid model, so it must be cleaned from the data. The CATIA® V5 R20 software has features which help to point out the noise from the data and with the help of a noise reduction tool the noise is reduced. After that, the 3D CAD model is prepared from the point cloud data. Figure 6 shows the 3D CAD model of the original (existing) disc CAM. The output of the point cloud processing phase is merged, cleaned, point cloud data set in the most convenient format. All the dimensions of the original (existing) disc CAM which was unknown can be easily obtained with the help of the 3D CAD model.

The observed results are obtained and calculated based on the data generated from this paper in the following sub-section.

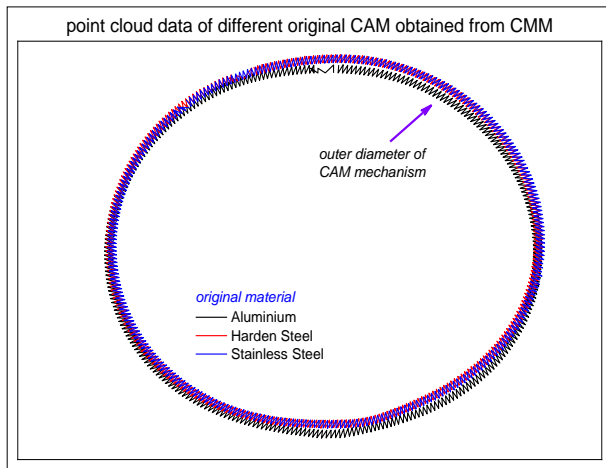


Fig. 5: Point Cloud Data of Different Origin (Existing) Disc CAM Obtained from CMM Machine

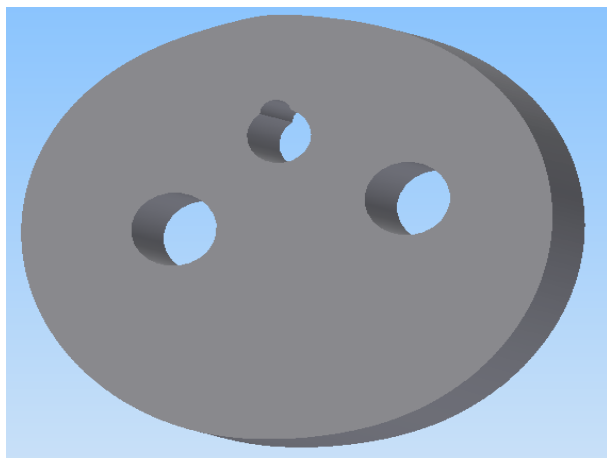


Fig. 6: 3D CAD Model of the Disc CAM.

### 3.1. Height variation assessment

Here, the height variation of all reversed disc CAMs including the original (existing) disc CAM was measured using an electronic digital Vernier calliper gauge (traditional measurement methods, especially as far as job-lot or individual production are concerned [36]) and calculation of the deviation relative to the original (existing) STL file format generated from CMM taking into consideration a tolerance dependant on the use of a surface. Figure 7 shows the nine points measured at each original (existing) and reversed disc CAM. All reversed disc CAMs show some height variation of the actual value of 10 mm height.

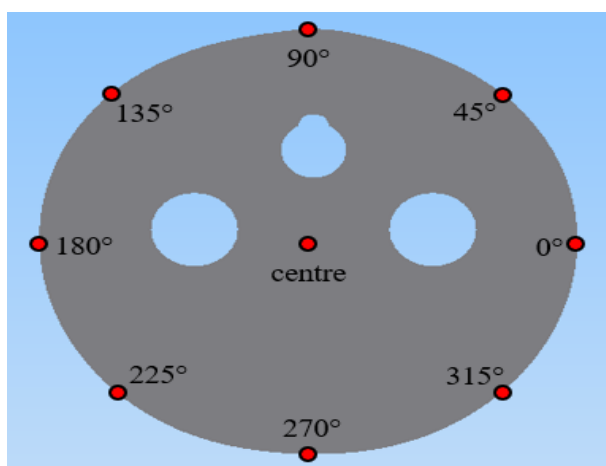


Fig. 7: Nine Measurement Location on Each Reversed and Original (Existing) Disc CAM

Figure 8 shows the dimensional variation between the original (existing) STL file format and printed parts in height. Figure 8(a) showed that the data obtained from the CMM machine for the original (existing) disc CAM revealed that the average value of the height variation for hardened steel and stainless steel were  $10.01 \pm 0.00$  mm and  $10.00 \pm 0.01$  mm, respectively, and it does show some height variation in the original aluminium disc CAM of around  $9.95 \pm 0.07$  mm. The maximum and minimum value of the average height variation over the original (existing) disc CAM profile was 10.01 mm and 9.80 mm with a total range of 0.21 mm (for aluminium), 10.01 mm and 10.00 mm with an entire range of 0.01 mm (for hardened steel) and 10.01 mm and 9.99 mm with a total range of 0.02 mm (for stainless steel).

In the case of manufacturing a reversed disc CAM of aluminium, hardened steel and stainless steel using CNC machine as shown in Figure 8(b), no shape errors occur in the final samples with mean and standard deviation (mean $\pm$ SD) of  $9.99 \pm 0.00$  mm,  $10.01 \pm 0.01$  mm and  $10.00 \pm 0.01$  mm, respectively, indicating that hardened steel and stainless steel reversed by almost 100%, whereas aluminium reversed by nearly 99.9% when using a CNC machine compared to the actual value of 10 mm. The maximum and minimum value of the average height variation over the reversed disc CAM profile was 9.99 mm and 9.98 mm with a total range of 0.01 mm (for STL file of aluminium), 10.02 mm and 9.99 mm with a complete range of 0.03 mm (for STL file of hardened steel) and 10.02 mm and 9.98 mm with a complete range of 0.04 mm (for STL file of stainless steel).

When using the 3D laser printer as shown in Figure 8(c), the form-labs black V1 resin was used for reversed disc CAM of the original (existing) STL file of aluminium, hardened steel and stainless steel. It shows some height variation with the mean and standard deviation (mean $\pm$ SD) of  $9.71 \pm 0.06$  mm,  $9.86 \pm 0.04$  mm and  $9.85 \pm 0.04$  mm, respectively, indicating that the reversed disc CAM was recovered by almost 97.1%, 98.6% and 98.5%, respectively. The maximum and minimum value of the average height variation over the reversed disc CAM profile was 9.84 mm and 9.63 mm with a total range of 0.21 mm (for STL file of aluminium), 9.93 mm and 9.81 mm with a full range of 0.12 mm (for STL file of hardened steel) and 9.91 mm and 9.78 mm with an entire range of 0.13 mm (for STL file of stainless steel).

The same procedure was followed with 3D FDM PLA+, 3D FDM PLA and 3D FDM ABS+. With PLA+ as shown in Figure 8(d), the mean and standard deviation (mean $\pm$ SD) of the original (existing) STL file of aluminium, hardened steel and stainless steel was  $9.87 \pm 0.02$  mm,  $9.95 \pm 0.04$  mm and  $9.90 \pm 0.02$  mm, respectively, indicating that almost 98.7%, 99.5% and 99.0%, respectively, recovered the reversed disc CAM. The maximum and minimum value of the average height variation over the reversed disc CAM profile was 9.91 mm and 9.85 mm with a total range of 0.06 mm (for STL file of aluminium), 10.00 mm and 9.90 mm with a total range of 0.10 mm (for an STL file of hardened steel) and 9.92 mm and 9.86 mm with a total range of 0.06 mm (for STL file of stainless steel).

With PLA as shown in Figure 8(e), the mean and standard deviation (mean $\pm$ SD) of the original (existing) STL file of aluminium, hardened steel and stainless steel was  $10.00 \pm 0.06$  mm,  $9.96 \pm 0.03$  mm and  $10.16 \pm 0.19$  mm, respectively, indicating that almost 100%, 99.6% and 101.6%, respectively, recovered the reversed disc CAM. The maximum and minimum value of the average height variation over the reversed disc CAM profile was 10.09 mm and 9.90 mm with a total range of 0.19 mm (for STL file of aluminium), 10.02 mm and 9.91 mm with a total range of 0.11 mm (for STL file of hardened steel) and 10.70 mm and 10.05 mm with a total range of 0.65 mm (for an STL file of stainless steel).

Finally, with ABS+ as shown in Figure 8(f), the mean and standard deviation (mean $\pm$ SD) of the original STL file of aluminium, hardened steel and stainless steel was  $9.87 \pm 0.17$  mm,  $9.85 \pm 0.16$  mm and  $9.99 \pm 0.18$  mm, respectively, indicating that almost 98.7%, 98.5% and 99.9%, respectively, recovered the reversed disc CAM. The maximum and minimum value of the average height variation over the reversed disc CAM profile was 10.23

mm and 9.55 mm with a total range of 0.68 mm (for STL file of aluminium), 10.03 mm and 9.57 mm with a total range of 0.46 mm (for STL file of hardened steel) and 10.33 mm and 9.73 mm with a total range of 0.60 mm (for STL file of stainless steel). It concluded that the ABS+ shows some warping deformation with high deviation from the original (existing) STL file of aluminum, hardened steel and stainless steel followed by formlabs black V1 resin (3D laser), 3D FDM PLA, 3D FDM PLA+ and CNC machine. This variation in height for the thermoplastic filament materials compared to the actual value of the original (existing) STL file might be due to the nozzle temperature of 220°C which is constant for all thermoplastic filament materials.

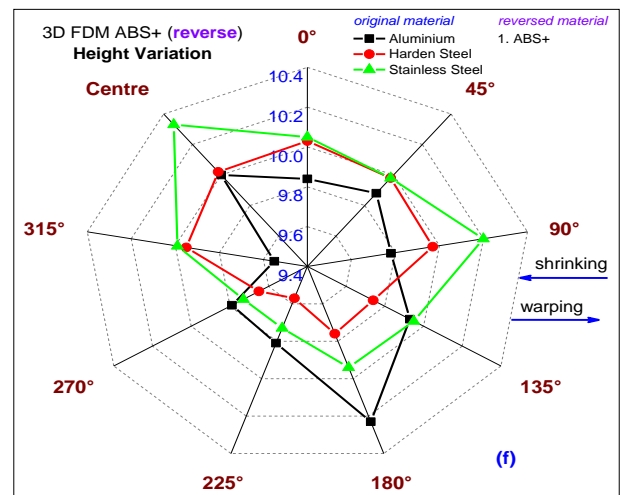
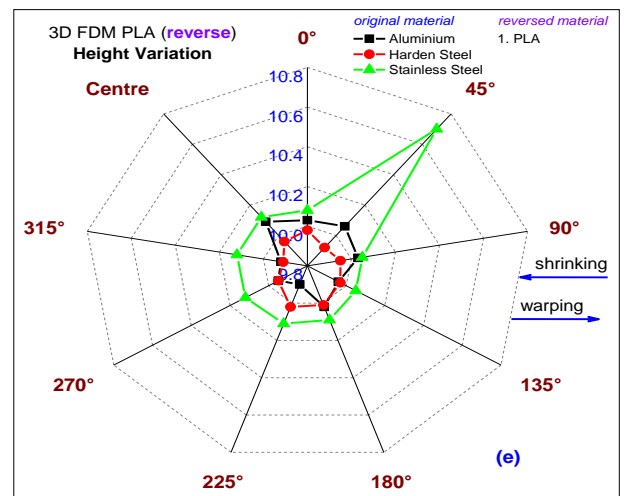
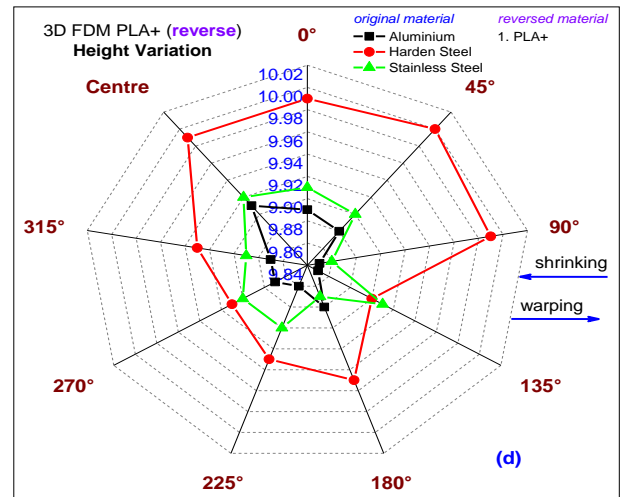
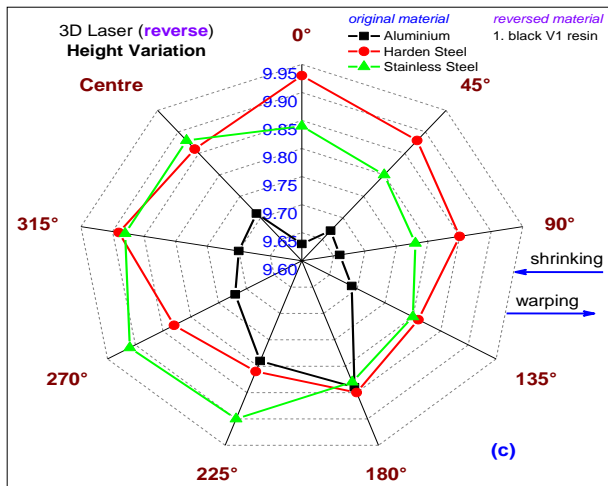
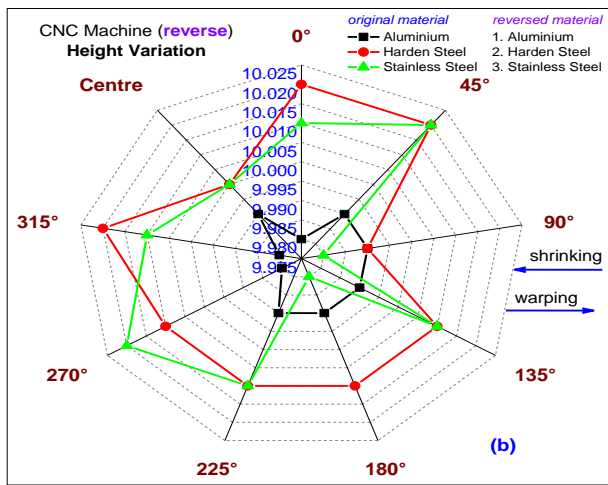
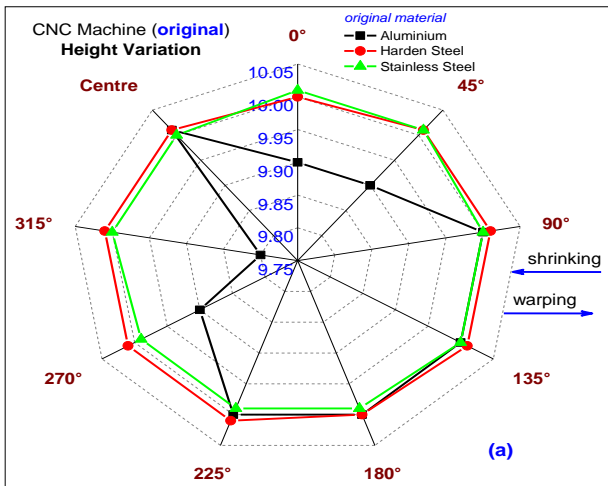
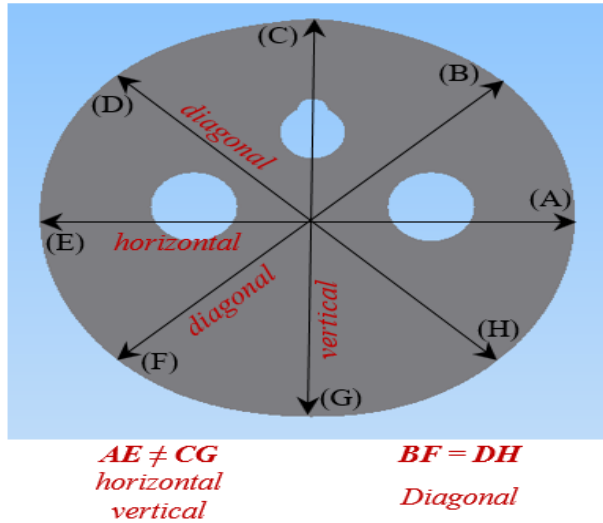


**Fig. 8:** Height Variation at Different Locations Over the Disc CAM of Aluminium, Hardened Steel and Stainless Steel (A) Original Disc CAM Manufactured by CNC Machine and (B) Reversed Disc CAM Manufactured by CNC Machine (C) Reversed Disc CAM Printed by 3D Laser (D) Reversed Disc CAM Printed by 3D FDM PLA+ (E) Reversed Disc CAM Printed by 3D FDM PLA and (F) Reversed Disc CAM Printed by 3D FDM ABS+.

### 3.2. Dimensional accuracy assessment

Similarly, the dimensional accuracy of all reversed and original (existing) disc CAMs was measured using an electronic digital Vernier caliper gauge and calculation of the deviation relative to the original (existing) STL file format. Figure 9 shows the dimensional accuracy measurement of the disc CAM in vertical, horizontal and diagonal axis, where BF and HD in the diagonal axis

are equal in distance, whereas, AE in the horizontal axis does not match CG in the vertical axis in terms of the distance because of the tip in the disc CAM at 90°. All reversed disc CAM show some differences in the dimensional accuracy compared to the actual values.

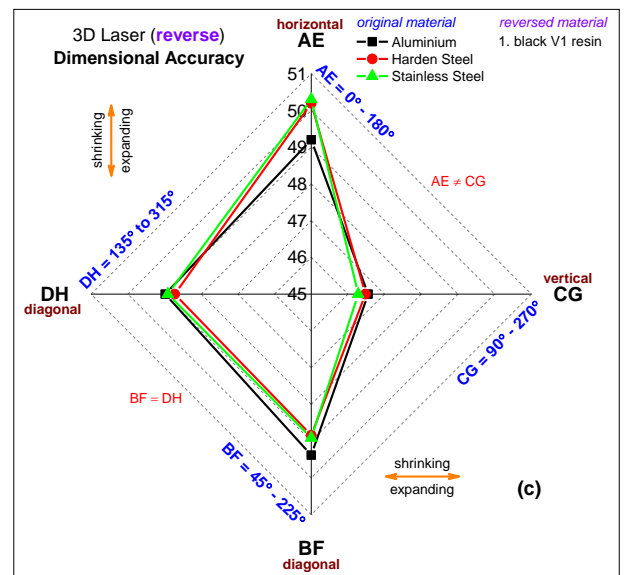
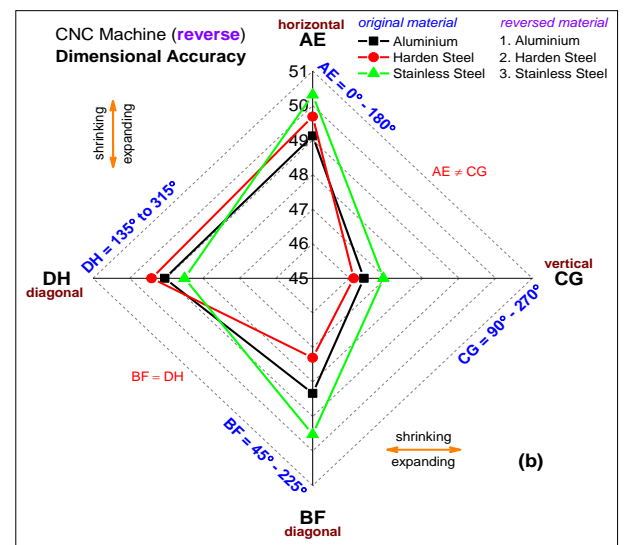
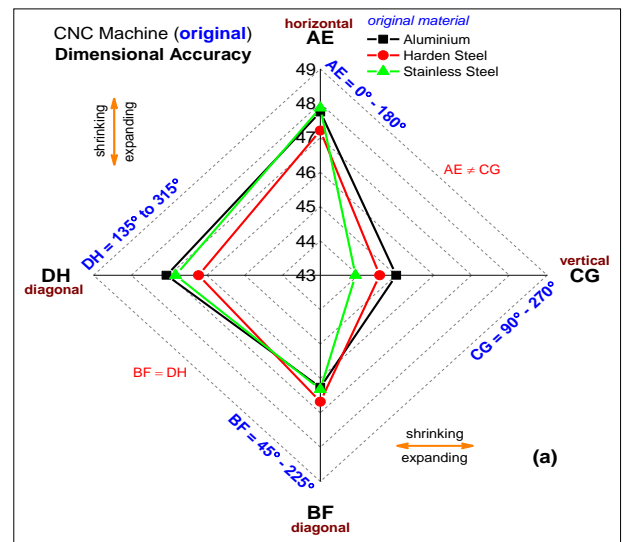


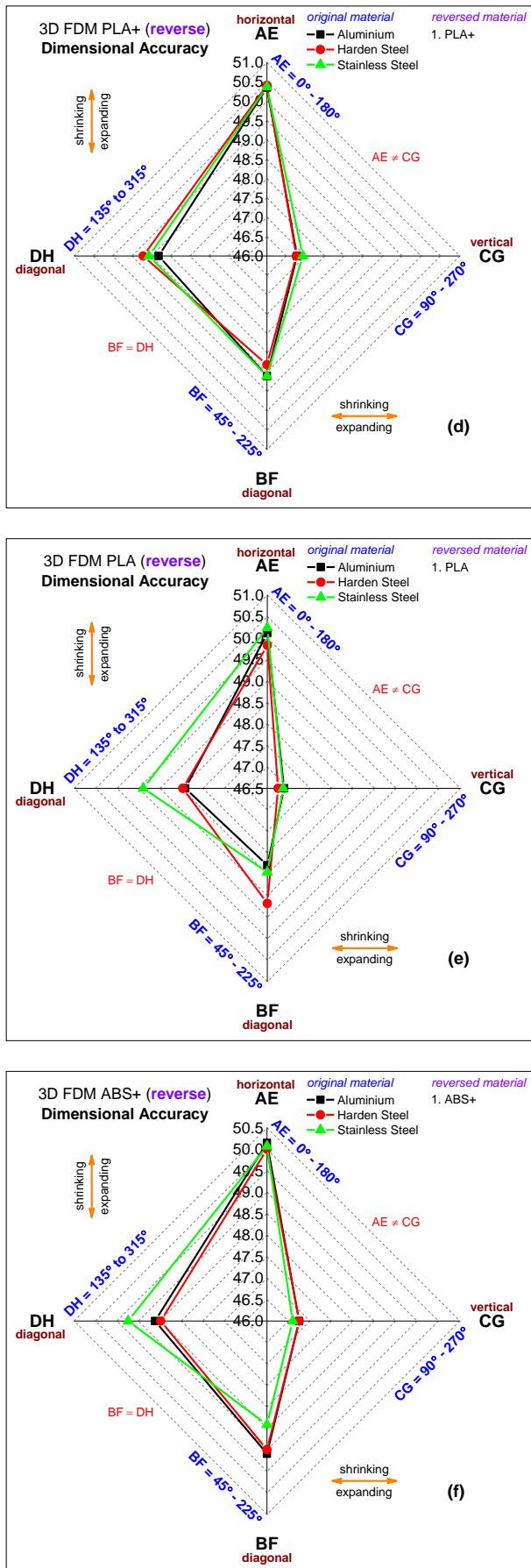
**Fig. 9:** Dimensional Accuracy Measurement of the Disc CAM in the Vertical, Horizontal and Diagonal Axis.

Figure 10 shows the dimensional variation between the original (disc CAM) STL file format and reversed disc CAM in height at nine different locations. As can be seen, all original (existing) and reversed disc CAMs follow the same hypothesis as the obtained data revealed that the AE (in the horizontal axis) does not match the CG (in the vertical axis) and BF (in the diagonal axis in one side) is equal in distance to the DH (in the diagonal axis in another side). The original (existing) materials of the disc CAM (aluminium, hardened steel, stainless steel) with the actual value which was measured by digital Vernier calliper and the CG = 45 mm (in the vertical axis), AE = 47 mm (in the horizontal axis) and BF and DH = 46 mm (in the diagonal axis).

Figures 10(b), 10(c), 10(d), 10(e) and 10(f) show the reversed disc CAM either manufactured by CNC machine or printed by 3D laser or 3D FDM printer. It also shows some differences in the dimensional accuracy of the actual value of 45 mm (vertical axis), 47 mm (horizontal axis) and 46 mm (diagonal axis). Clearly, in the vertical axis (CG) and horizontal axis (AE), there are surpluses in dimension by almost 4% to 6% from the original (existing) STL file of the disc CAM. Whereas, in the diagonal axis (BF and DH), there is more deviation from the actual value of the original (existing) STL file of the disc CAM by almost 3% to 7%. The maximum deviation occurs in the production of ABS+ printed by the 3D FDM printer in the vertical axis (CG) and horizontal axis (AE) for the reversed disc CAM of the STL file of stainless steel. The minimum deviation occurs in the production of hardened steel manufactured by the CNC machine in the diagonal axis (BF) for reversed disc CAM of STL file of hardened steel. This deviation from the actual value in the thermoplastic filament materials indicates that high warping deformation and dimensional variation occurs in these materials as the shrinkage or expansion is quite visible even when using the same material for reversing the disc CAM, the same dimensional variation occurs as well. Also, there is a non-uniform distribution in dimensional variation for both PLA and ABS+, which in diverting from the original (existing) STL file of aluminum, steel and stainless steel disc CAM. PLA+ shows less dimensional variation with the same independent variables followed by formlabs black V1 resin.

It also shows that there is no shrinking occurring in all reversed disc CAM in any axis but expanding shows otherwise in each axis.





**Fig. 10:** Dimensional Accuracy of the Disc CAM of Aluminium, Hardened Steel and Stainless Steel (A) Original Disc CAM Manufactured by CNC Machine and (B) Reversed Disc CAM Manufactured by CNC Machine (C) Reversed Disc CAM Printed by 3D Laser (D) Reversed Disc CAM Printed by 3D FDM PLA+ (E) Reversed Disc CAM Printed by 3D FDM PLA and (F) Reversed Disc CAM Printed by 3D FDM ABS+.

### 3.3. Surface roughness assessment

Figure 11 showed the measured surface profile values for each position of the original (existing) disc CAM (including aluminium, hardened steel and stainless steel) and reversed engineering disc CAM (including aluminium, hardened steel, stainless steel, PLA+, PLA, ABS+ and formlabs black V1 resin) and considering surface roughness,  $R_a$  value was calculated. It is worth mentioning that the measured locations of the  $R_a$  over the disc CAM profile were consistent with the same location for the height variation and dimensional accuracy measurements.

Based on the experimental data obtained from this research, variations in  $R_a$  profile distribution curves caused by different materials, manufacturing process parameters irregular steps and micro-sized burrs were observed. Thus, the actual surface profile distribution of reversed disc CAM compared with original (existing) disc CAM was influenced by several factors and conditions such as the build style and material property.

In general, the  $R_a$  values for the original (existing) disc CAM (including aluminium, hardened steel and stainless steel) and reversed engineering disc CAM (including aluminium, hardened steel, stainless steel) manufactured by CNC machine follows the same pattern all over the contact line including the tip at 90° which represents the highest surface roughness,  $R_a$ , by almost ~3  $\mu\text{m}$  compared with reset of the disc CAM profile. This tip is usually the starting and ending point of the cutting process during the CNC machine.

The  $R_a$  values for the reversed engineering disc CAM (including PLA+, PLA, ABS+ and formlabs black V1 resin) manufactured by the 3D laser printer and 3D FDM printer showed irregularity surface roughness distribution all over the contact line including the tip at 90° due to the samples of different filament materials being printed with a raster road of +45/-45 (diamond), 0/90 flat build orientation and 100% infill density pattern shape. The  $R_a$  value of the 3D laser peaked at ~7.5  $\mu\text{m}$  and increased by ~60% of the original (existing) disc CAM, the  $R_a$  value of 3D FDM PLA+ peaked at ~10  $\mu\text{m}$  and increased by ~70% of the original (existing) disc CAM, the  $R_a$  value of 3D FDM PLA peaked at ~12  $\mu\text{m}$  and increased by ~75% of the original (existing) disc CAM, the  $R_a$  value of 3D FDM ABS+ peaked at ~21  $\mu\text{m}$  and increased by ~85% of the original (existing) disc CAM. So, it can be concluded that the CNC machine follows the same original (disc CAM) STL file format reversed disc CAM in height variation at nine different locations for the same material (including aluminium, hardened steel, stainless steel), whereas, different behaviour was observed on the  $R_a$  when using thermoplastic materials such as PLA+, PLA, ABS+ and formlabs black V1 resin (photo-polymer). It therefore becomes clear that the solidification process which is more likely to be associated with nozzle temperature during printing needs a lot more time to heal and also needs a high nozzle temperature to fully stabilize at the new temperature setting and cool down slowly.

In Figure 11(a), the maximum and minimum value of the average surface roughness over the original (existing) disc CAM profile was 3.26  $\mu\text{m}$  and 0.61  $\mu\text{m}$  with a total range of 2.65  $\mu\text{m}$  (for aluminium), 3.23  $\mu\text{m}$  and 0.30  $\mu\text{m}$  with an entire range of 2.93  $\mu\text{m}$  (for hardened steel) and 2.97  $\mu\text{m}$  and 0.65  $\mu\text{m}$  with a full range of 2.32  $\mu\text{m}$  (for stainless steel).

In Figure 11(b), the maximum and minimum value of the average surface roughness over the reversed disc CAM profile of the aluminium, hardened steel and stainless steel was 2.88  $\mu\text{m}$  and 1.30  $\mu\text{m}$  with a total range of 1.58  $\mu\text{m}$  (for STL file of aluminium), 2.80  $\mu\text{m}$  and 0.75  $\mu\text{m}$  with a whole range of 2.05  $\mu\text{m}$  (for STL file of hardened steel) and 2.79  $\mu\text{m}$  and 0.64  $\mu\text{m}$  with an entire range of 2.15  $\mu\text{m}$  (for STL file stainless steel).

In Figure 11(c), the maximum and minimum value of the average surface roughness over the reversed disc CAM profile of the black V1 resin material was 7.32  $\mu\text{m}$  and 1.50  $\mu\text{m}$  with a total range of 5.82  $\mu\text{m}$  (for STL file of aluminium), 3.23  $\mu\text{m}$  and 1.17  $\mu\text{m}$  with an entire range of 2.06  $\mu\text{m}$  (for STL file of hardened steel) and

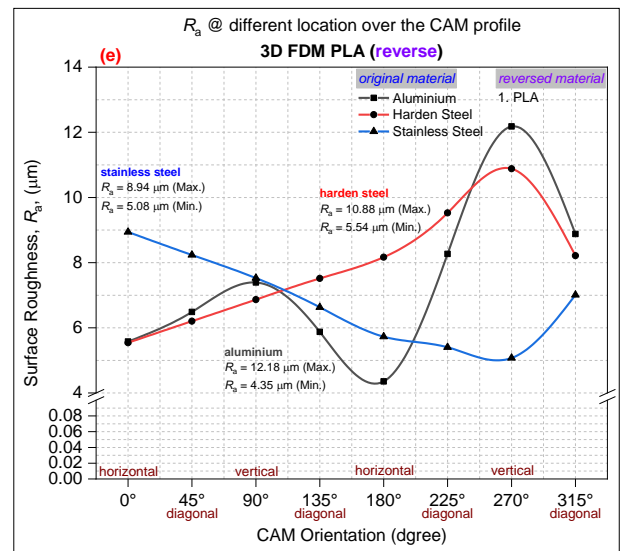
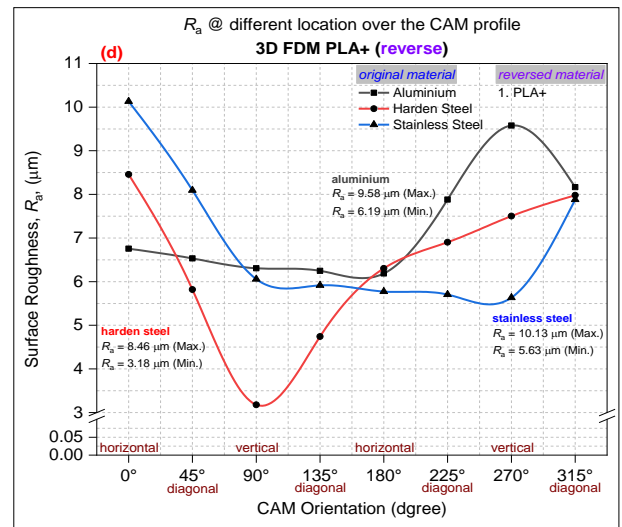
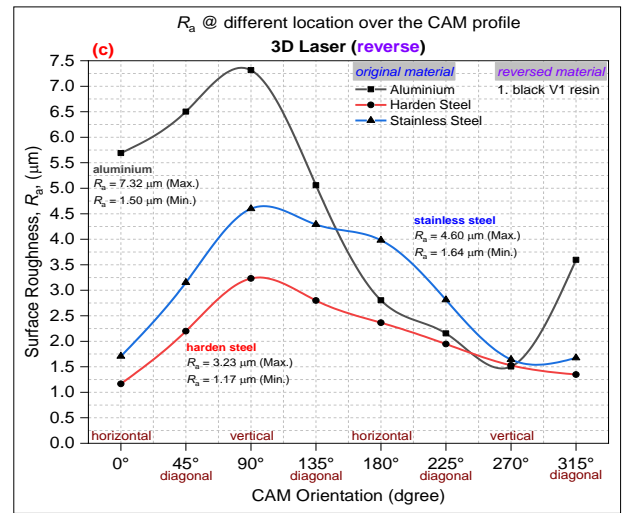
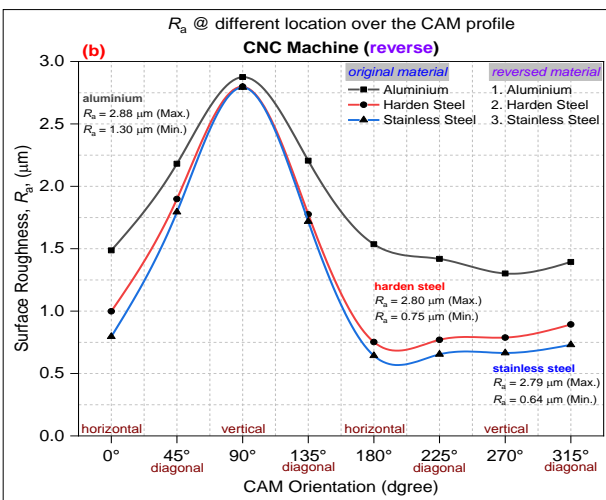
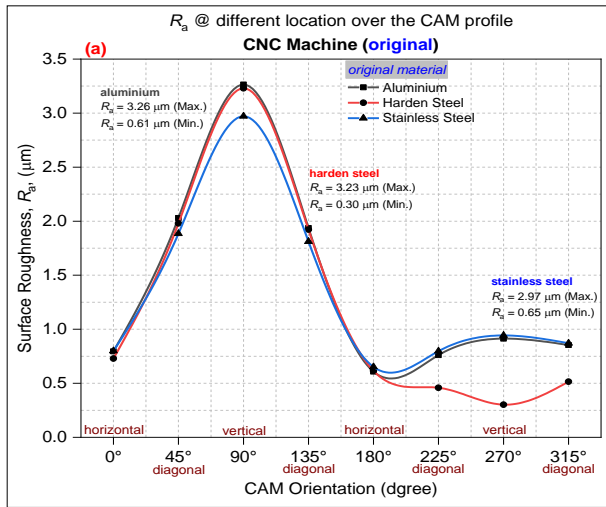
4.60  $\mu\text{m}$  and 1.64  $\mu\text{m}$  with a complete range of 2.96  $\mu\text{m}$  (for STL file of stainless steel).

In Figure 11(d), the maximum and minimum value of the average surface roughness over the reversed disc CAM profile of the PLA+ material was 9.58  $\mu\text{m}$  and 6.19  $\mu\text{m}$  with a total range of 3.39  $\mu\text{m}$  (for STL file of aluminium), 8.46  $\mu\text{m}$  and 3.18  $\mu\text{m}$  with a whole range of 5.28  $\mu\text{m}$  (for STL file of hardened steel) and 10.13  $\mu\text{m}$  and 5.63  $\mu\text{m}$  with a full range of 4.50  $\mu\text{m}$  (for STL file of stainless steel).

In Figure 11(e), the maximum and minimum value of the average surface roughness over the reversed disc CAM profile of the PLA material was 12.18  $\mu\text{m}$  and 4.35  $\mu\text{m}$  with a total range of 7.83  $\mu\text{m}$  (for STL file of aluminium), 10.88  $\mu\text{m}$  and 5.54  $\mu\text{m}$  with a full range of 5.34  $\mu\text{m}$  (for STL file of hardened steel) and 8.94  $\mu\text{m}$  and 5.08  $\mu\text{m}$  with a whole range of 3.86  $\mu\text{m}$  (for STL file of stainless steel).

In Figure 11(f), the maximum and minimum value of the average surface roughness over the reversed disc CAM profile of the ABS+ material was 20.19  $\mu\text{m}$  and 6.15  $\mu\text{m}$  with a total range of 14.04  $\mu\text{m}$  (for STL file of aluminium), 8.29  $\mu\text{m}$  and 4.01  $\mu\text{m}$  with a complete range of 4.28  $\mu\text{m}$  (for STL file of hardened steel) and 18.17  $\mu\text{m}$  and 8.29  $\mu\text{m}$  with an entire range of 9.88  $\mu\text{m}$  (for STL file of stainless steel).

To conclude, for all reversed disc CAMs, the high peak or deep valley over the disc CAM profile will play a significant role in the directions of reciprocating movements, particularly at small-scale displacement. The original (existing) and reversed disc CAM of the same materials follow the same pattern, whereas, the thermo-plastic filament materials showed non-uniform surface roughness distribution between the peaks and valleys, which will affect the maximum and minimum micro- and nano-scale follower displacement.



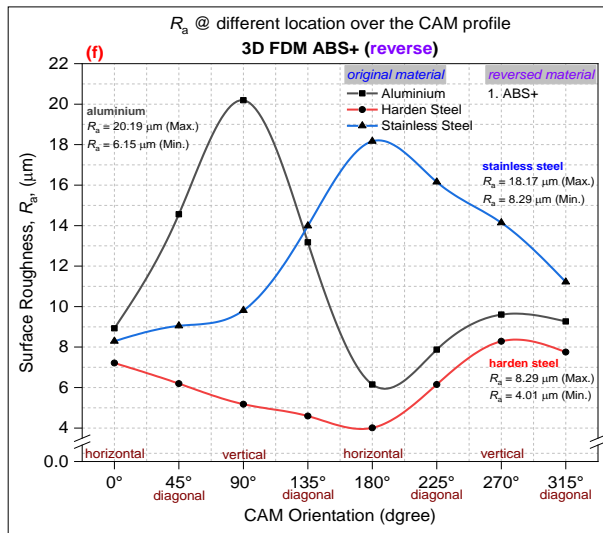


**Fig. 11:** Surface Roughness at Different Locations Over the Disc CAM of Aluminium, Hardened Steel and Stainless Steel (A) Original Disc CAM Manufactured by CNC Machine (B) Reversed Disc CAM Manufactured by CNC Machine (C) Reversed Disc CAM Printed by 3D Laser (D) Reversed Disc CAM Printed by 3D FDM PLA+ (E) Reversed Disc CAM Printed by 3D FDM PLA and (F) Reversed Disc CAM Printed by 3D FDM ABS+.

Figure 12 shows the average surface roughness values over the disc CAM. The mean and standard deviation (mean±SD) of the surface roughness measured over the original (existing) disc CAM was  $1.40 \pm 0.93 \mu\text{m}$  (for aluminium),  $1.22 \pm 1.04 \mu\text{m}$  (for hardened steel) and  $1.34 \pm 0.81 \mu\text{m}$  (for stainless steel), indicating that the disc CAM of aluminium manufactured by CNC was rougher than hardened steel and stainless steel by approximately ~13% and ~4%, respectively.

For reversed CAM manufactured by the CNC machine using the same engineering materials as the original (existing) disc CAM, the mean and standard deviation (mean±SD) of the surface roughness measured over the reversed disc CAM was  $1.80 \pm 0.56 \mu\text{m}$  (for aluminium),  $1.33 \pm 0.75 \mu\text{m}$  (for hardened steel) and  $1.22 \pm 0.80 \mu\text{m}$  (for stainless steel), indicating that the disc CAM of aluminium manufactured by CNC was rougher than hardened steel and stainless steel again by approximately ~26% and ~32%, respectively. Reversing the disc CAM using aluminium and hardened steel, the surface roughness increased by almost ~29% and ~9%, respectively, whereas, the stainless steel decreased by nearly ~9%.

For reversed disc CAM printed by 3D laser using black V1 resin (photo-polymer) material, the mean and standard deviation (mean±SD) of the surface roughness measured over the reversed disc CAM was  $4.33 \pm 2.13 \mu\text{m}$  (for aluminium),  $2.07 \pm 0.72 \mu\text{m}$  (for hardened steel) and  $2.98 \pm 1.23 \mu\text{m}$  (for stainless steel), indicating that the disc CAM of black V1 resin obtained from STL file of aluminium and printed by 3D laser was rougher than the black V1 resin obtained from STL file of hardened steel and black V1 resin obtained from STL file of stainless steel again by approximately ~52% and ~31%, respectively. Reversing the disc CAM using an STL file of aluminium, hardened steel and stainless steel, the surface roughness increased by almost ~209%, ~70% and 122%, respectively.

For the reversed disc CAM printed by 3D FDM using PLA+ thermoplastic filament material, the mean and standard deviation (mean±SD) of the surface roughness measured over the reversed disc CAM was  $7.21 \pm 1.22 \mu\text{m}$  (for aluminium),  $6.36 \pm 1.76 \mu\text{m}$  (for hardened steel) and  $6.90 \pm 1.64 \mu\text{m}$  (for stainless steel), indicating that the disc CAM of PLA+ obtained from STL file of aluminium and printed by 3D FDM was rougher than PLA+ obtained from STL file of hardened steel and PLA+ obtained from STL file of stainless steel by approximately ~12% and ~4%, respectively. Reversing the disc CAM using an STL file of aluminium, hardened steel and stainless steel, the surface roughness increased by

almost ~415%, ~421% and 415%, respectively, which means that the surface roughness of the reversed disc CAM profile was four times rougher than the original (existing) disc profile.

For reversed disc CAM printed by 3D FDM using PLA thermoplastic filament material, the mean and standard deviation (mean±SD) of the surface roughness measured over the reversed disc CAM was  $7.38 \pm 2.44 \mu\text{m}$  (for aluminium),  $7.86 \pm 1.75 \mu\text{m}$  (for hardened steel) and  $6.82 \pm 1.38 \mu\text{m}$  (for stainless steel), indicating that the disc CAM of PLA+ obtained from an STL file of hardened steel and printed by 3D FDM was rougher than PLA+ obtained from an STL file of aluminium and PLA+ obtained from an STL file of stainless steel by approximately ~6% and ~13%, respectively. Reversing the disc CAM using an STL file of aluminium, hardened steel and stainless steel, the surface roughness of PLA increased by almost ~427%, ~544% and 409%, respectively, which means that the surface roughness of the reversed disc CAM profile was four times rougher for aluminium and stainless steel and five times rougher for the hardened steel than the original (existing) disc profile.

For the reversed disc CAM printed by 3D FDM using ABS+ thermoplastic filament material, the mean and standard deviation (mean±SD) of the surface roughness measured over the reversed disc CAM was  $11.22 \pm 4.54 \mu\text{m}$  (for aluminium),  $6.17 \pm 1.52 \mu\text{m}$  (for hardened steel) and  $12.60 \pm 3.56 \mu\text{m}$  (for stainless steel), indicating that the disc CAM of ABS+ obtained from STL file of stainless steel and printed by 3D FDM was rougher than ABS+ obtained from an STL file of aluminium and ABS+ obtained from an STL file of hardened steel by approximately ~11% and ~51%, respectively. Reversing the disc CAM using an STL file of aluminium, hardened steel and stainless steel, the surface roughness of ABS+ increased by almost ~701%, ~406% and 842%, respectively.

In general, the reversed disc CAM of stainless steel manufactured by CNC represents the lowest surface roughness as it decreased by 9% from the original (existing) STL file of stainless steel. On the other hand, the reversed disc CAM of ABS+ obtained from the original (existing) STL file of stainless steel represents the roughest surface roughness as it was increased almost eightfold compared to the original (existing) STL file. It is worth mentioning that the PLA+ and PLA thermoplastic filament materials showed the very similar behaviour of the surface roughness of around a 400% increase from the original (existing) STL file aluminium, hardened steel and stainless steel. Furthermore, it shows clearly that the standard deviation (±SD) showed best results in a range from  $\pm 0.56$  to  $\pm 1.04 \mu\text{m}$  for both original (existing) and reversed disc CAM of aluminium, hardened steel and stainless steel.

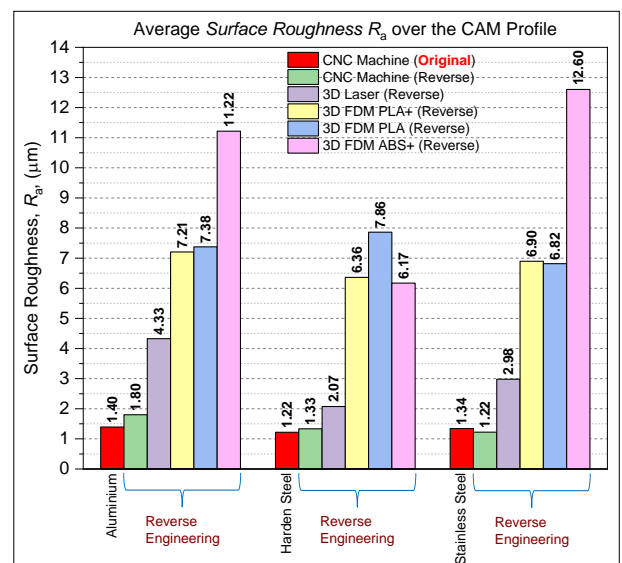


**Fig. 12:** Average Surface Roughness over the Original (Existing) Disc CAM of Aluminium, Hardened Steel and Stainless Steel and the Reversed Disc CAM.

### 3.4. Skewness vs. kurtosis assessment

The surface topology was studied with the surface asymmetry (skewness,  $R_{sk}$ ) and the coefficient of its inclination (kurtosis,  $R_{ku}$ ) in all samples (the original STL file of the disc CAM of aluminium, hardened steel, stainless steel) and (the reversed disc CAM including aluminium, hardened steel, stainless steel, PLA+, PLA, ABS+ and formlabs black V1 resin). This step of the study is vital to predict the functional behaviour of the disc CAM profile before and after reversal, such as tribological properties of the surface (which involves the study of the friction coefficient and wear rate of different materials, see [37-39]).

Figure 13 showed the skewness,  $R_{sk}$ , 3<sup>rd</sup> moment versus the kurtosis,  $R_{ku}$ , 4<sup>th</sup> moment of all original (existing) and reversed disc CAMs. Ideally, a value of zero for skewness ( $R_{sk} = 0$ ) and a value of three for kurtosis ( $R_{ku} = 3$ ) is typical for a random, accurate Gaussian profile and weakly isotropic. For asymmetric height distribution, the skewness,  $R_{sk}$ , can be negative or positive values ( $R_{sk} > 0$  for steep peaks and flat valleys (positively skewed distribution) whereas  $R_{sk} < 0$  for flat peaks and steep valleys (negatively skewed distribution)). A profile with sharper peaks (spiky) has the value of  $R_{ku} > 3$  (leptokurtic, homogeneous and narrow scatter). In contrast,  $R_{ku} < 3$  (platykurtic, heterogeneous and wide spread) indicates a disc CAM profile distribution with round, bumpy and less frequent peaks. Incidentally, data is provided on the real contact area and wear resistance. Also, it is likely to detect the periodicity of the profile distribution  $R_{ku} < 3$ .

Figure 13(a) shows that the plot of  $R_{sk}$  (3<sup>rd</sup> moment) against  $R_{ku}$  (4<sup>th</sup> moment) of the original (existing) STL file of the disc CAM profile of aluminium, hardened steel and stainless steel is centred around the random Gaussian profile, which was the negatively skewed distribution and positively skewed distribution and leptokurtic distribution and platykurtic distribution with a low and high degree of peakedness. It shows that the general trend of the positive skewness and negative skewness is not equally distributed over all the three original (existing) STL files of the disc CAM, which is more likely to be positively skewed than negatively skewed. The maximum and minimum trend of skewness and kurtosis was in the region of  $-0.84 \leq R_{sk} \leq 1.3$  (60.7% positively skewed distribution and 39.3% negatively skewed distribution) and  $1.46 \leq R_{ku} \leq 6.85$  (17.6% platykurtic distribution with a low degree of peakedness and 82.4% leptokurtic distribution with a high degree of peakedness) with a range of 2.14 and 5.39 for  $R_{sk}$  and  $R_{ku}$ , respectively. After using regression analysis, the R-squared values was 0.7 (for aluminum), 0.7 (for hardened steel) and 0.9 (for stainless steel).

Figure 13(b) shows  $R_{sk}$  against  $R_{ku}$  performance for the reversed disc CAM of aluminum, hardened steel and stainless steel machined by CNC machine. It shows that the general trend of the positive skewness and negative skewness is equally distributed except the reversed disc CAM of aluminum was shifted from positive skewness to 100% negative skewness. The maximum and minimum trend of skewness and kurtosis was in the region of  $-0.91 \leq R_{sk} \leq 0.54$  (37.2% positively skewed distribution and 62.8% negatively skewed distribution) and  $1.72 \leq R_{ku} \leq 4.81$  (26.3% platykurtic distribution with a low degree of peakedness and 73.6% leptokurtic distribution with high degree of peakedness) with a range of 1.45 and 3.09 for  $R_{sk}$  and  $R_{ku}$ , respectively. After using regression analysis, the R-squared values was 0.5 (for reversed aluminum), 1.0 (for reversed hardened steel) and 0.3 (for reversed stainless steel).

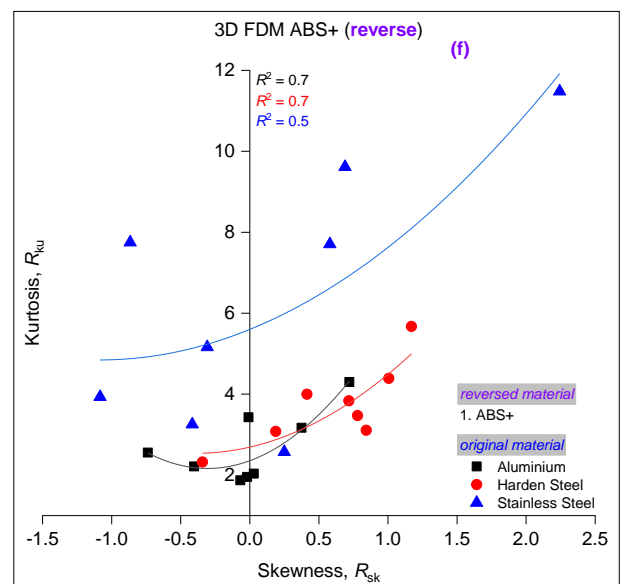
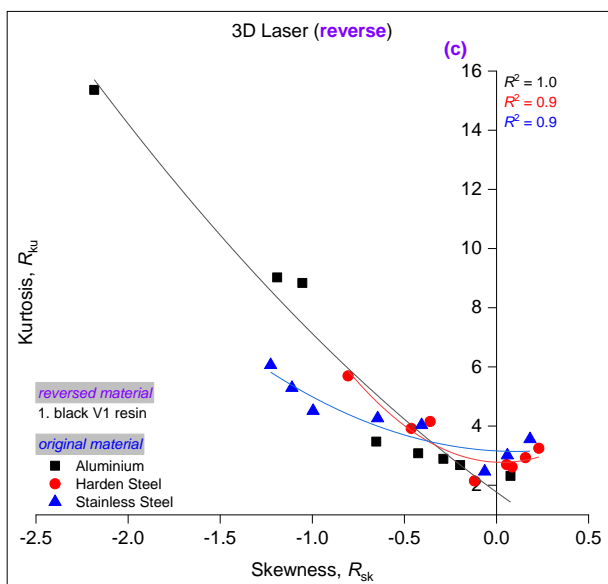
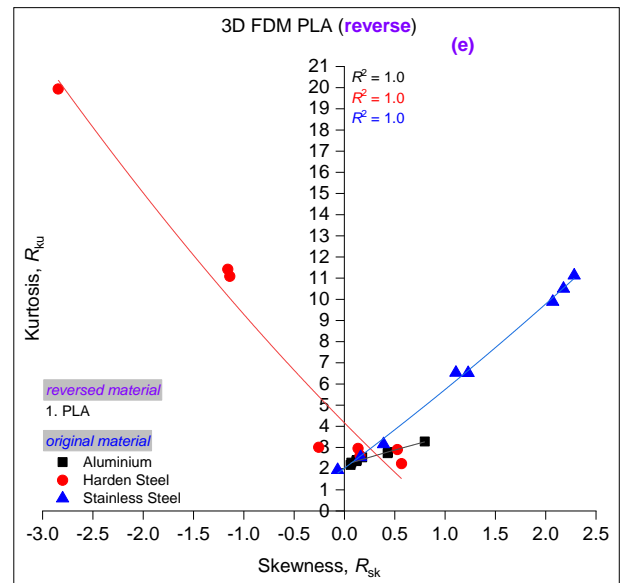
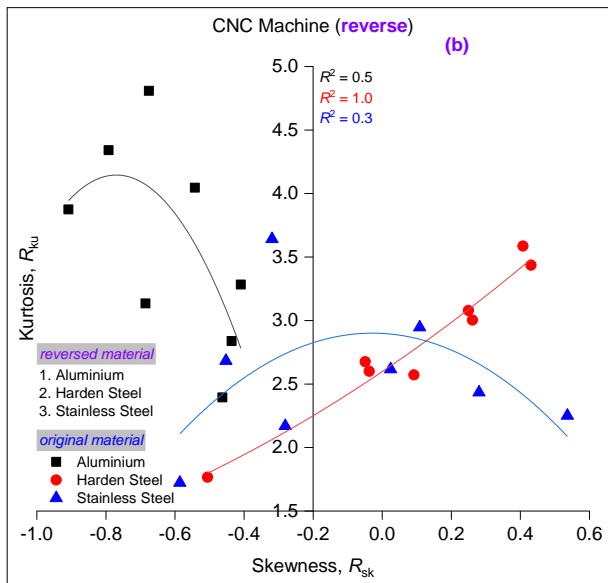
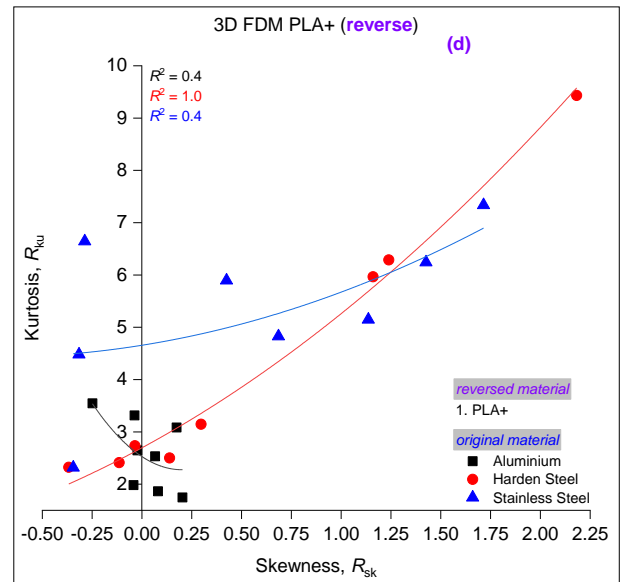
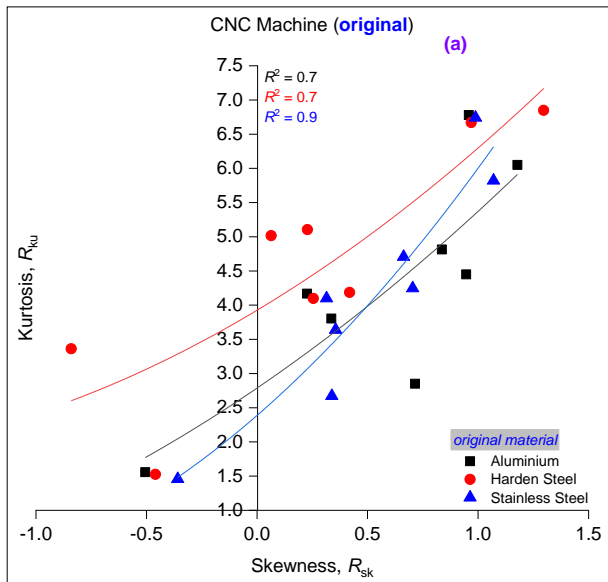
Figure 13(c) shows  $R_{sk}$  against  $R_{ku}$  performance for reversed disc CAM of formlabs black V1 resin (photo-polymer) printed by a 3D laser printer. The general trend showed positive skewness (+ve for steep peaks and flat valleys) and negative skewness (-ve for flat peaks and steep valleys) but not equal distribution of this between them but rather a tendency to be negatively skewed than positively skewed as regards the surface roughness. Surprisingly, the formlabs black V1 resin reversed from an aluminum sample remaining with almost 99% negative skewness. The maximum and minimum trend of skewness and kurtosis was in the region of  $-2.18 \leq R_{sk} \leq$

0.23 (9.5% positively skewed distribution and 90.5% negatively skewed distribution) and  $2.15 \leq R_{ku} \leq 5.70$  (27.4% platykurtic distribution with a low degree of peakedness and 72.6% leptokurtic distribution with a high degree of peakedness) with a range of 2.41 and 3.55 for  $R_{sk}$  and  $R_{ku}$ , respectively. After using regression analysis, the R-squared values were 1.0 (for reversed aluminum), 0.9 (for reversed hardened steel) and 0.9 (for reversed stainless steel).

Figure 13(d) shows  $R_{sk}$  against  $R_{ku}$  performance for reversed disc CAM of PLA+ printed by a 3D FDM printer. The general trend showed positive skewness (+ve for steep peaks and flat valleys) and negative skewness (-ve for flat peaks and steep valleys) but not equal distribution of this between them but rather a tendency to be positively skewed than negatively skewed as regards the surface roughness which is more likely to be the reversed behaviour of formlabs black V1 resin. The maximum and minimum trend of skewness and kurtosis was in the region of  $-0.37 \leq R_{sk} \leq 2.18$  (85.5% positively skewed distribution and 14.5% negatively skewed distribution) and  $1.75 \leq R_{ku} \leq 9.43$  (15.7% platykurtic distribution with a low degree of peakedness and 84.3% leptokurtic distribution with a high degree of peakedness) with a range of 2.55 and 7.68 for  $R_{sk}$  and  $R_{ku}$ , respectively. After using regression analysis, the R-squared values was 0.4 (for reversed aluminum), 1.0 (for reversed hardened steel) and 0.4 (for reversed stainless steel).

Figure 13(e) shows  $R_{sk}$  against  $R_{ku}$  performance for reversed disc CAM of PLA printed by a 3D FDM printer. It shows that the general trend of the positive skewness and negative skewness is equally distributed for PLA reversed by hardened steel except for the fact that the reversed disc CAM of aluminum stainless steel was shifted from a negative skewness to 100% and 99% negative skewness, respectively. The maximum and minimum trend of skewness and kurtosis was in the region of  $-2.85 \leq R_{sk} \leq 2.28$  (44.4% positively skewed distribution and 55.6% negatively skewed distribution) and  $1.94 \leq R_{ku} \leq 19.9$  (8.88% platykurtic distribution with low degree of peakedness and 45.7% leptokurtic distribution with high degree of peakedness) with a range of 5.13 and 18 for  $R_{sk}$  and  $R_{ku}$ , respectively. After using regression analysis, the R-squared values was 1.0 (for reversed aluminum), 1.0 (for reversed hardened steel) and 1.0 (for reversed stainless steel) with 100% level of confidence and coverage factor,  $k = 3$ .

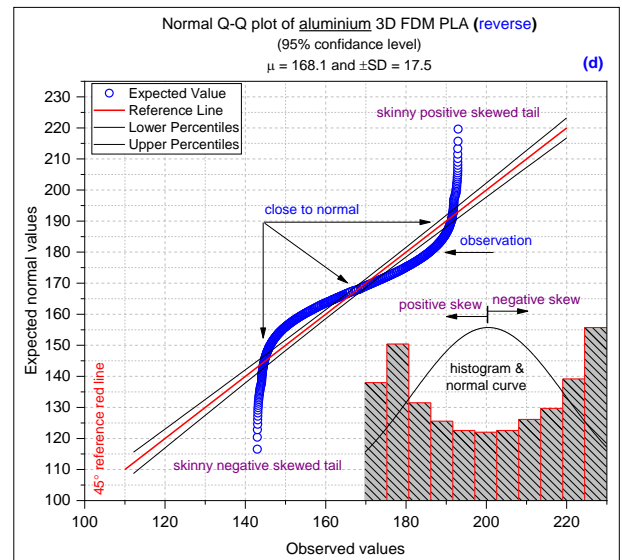
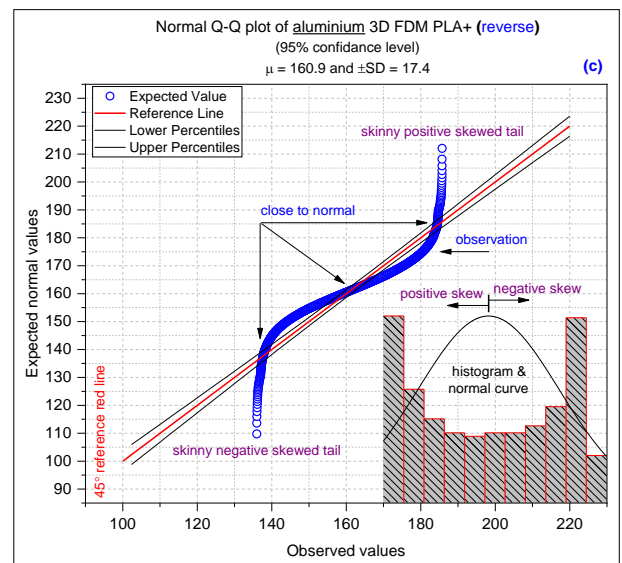
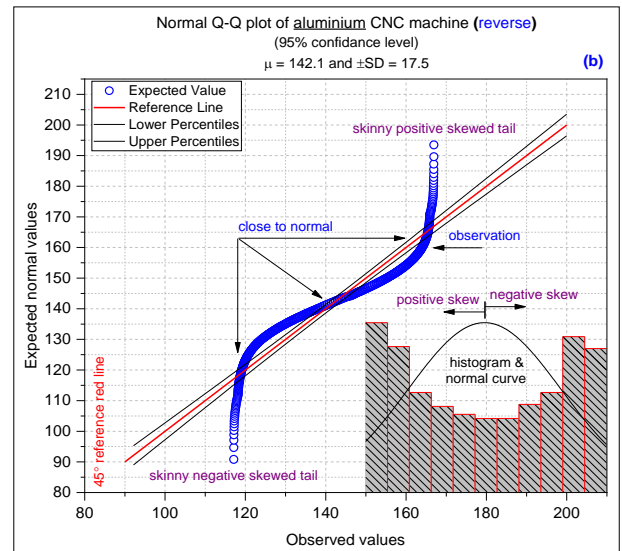
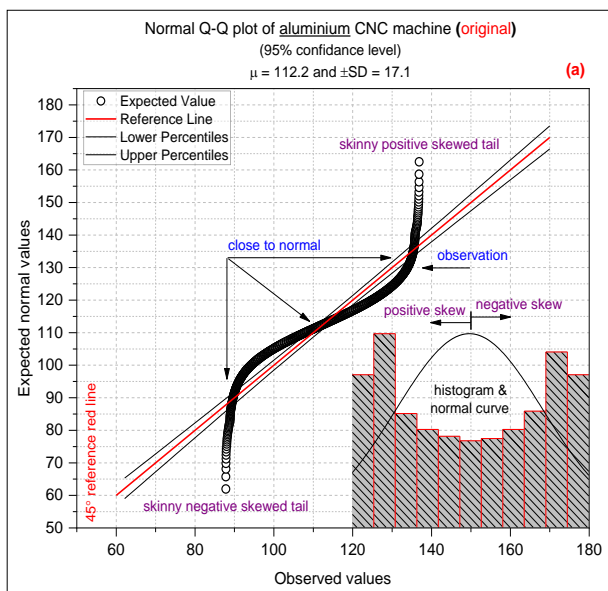
Figure 13(f) shows  $R_{sk}$  against  $R_{ku}$  performance for reversed disc CAM of ABS+ printed by 3D FDM printer. It shows that the general trend of the positive skewness and negative skewness is equally distributed for ABS+ reversed by aluminum, hardened steel and stainless steel. The maximum and minimum trend of skewness and kurtosis was in the region of  $-1.08 \leq R_{sk} \leq 2.24$  (67.5% positively skewed distribution and 32.5% negatively skewed distribution) and  $1.87 \leq R_{ku} \leq 11.4$  (14.1% platykurtic distribution with low degree of peakedness and 85.9% leptokurtic distribution with high degree of peakedness) with a range of 3.32 and 9.53 for  $R_{sk}$  and  $R_{ku}$ , respectively. After using regression analysis, the R-squared values was 0.7 (for reversed aluminum), 0.7 (for reversed hardened steel) and 0.5 (for reversed stainless steel).

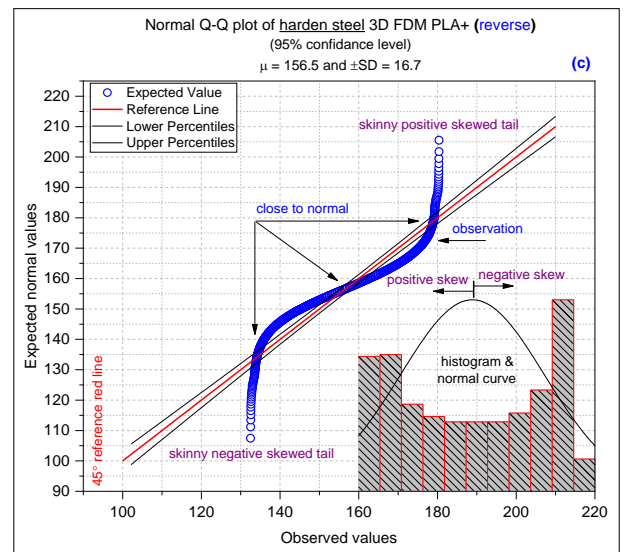
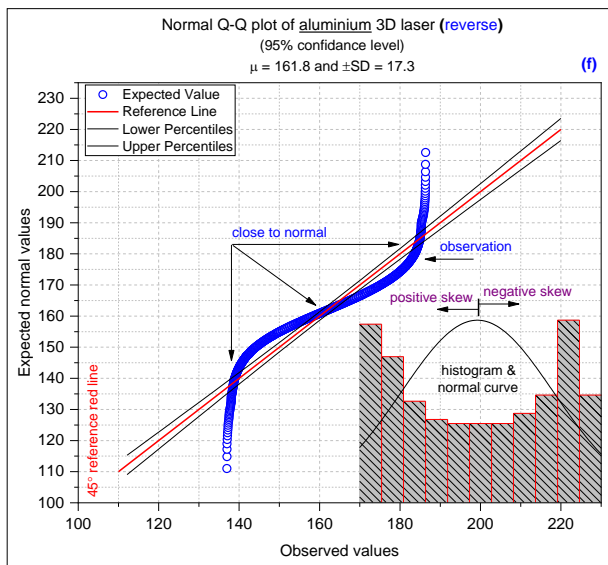
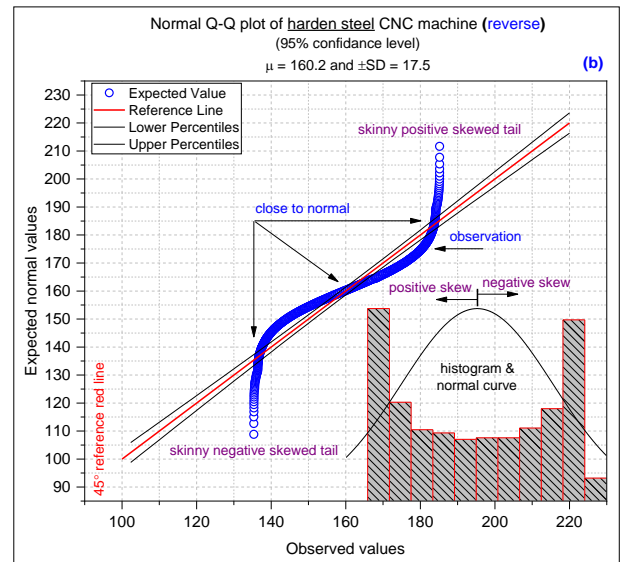
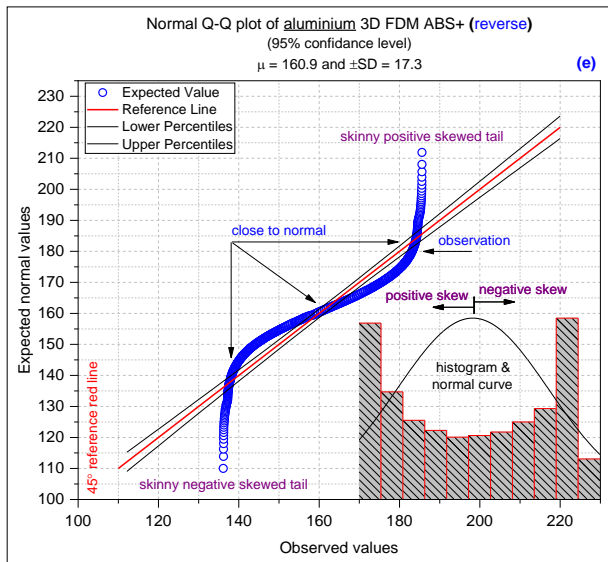


**Fig. 13:** Skewness vs. Kurtosis (A) Original Disc CAM Manufactured by A CNC Machine and (B) Reversed Disc CAM Manufactured by CNC Machine (C) Reversed Disc CAM Printed by A 3D Laser (D) Reversed Disc CAM Printed by A 3D FDM PLA+ (E) Reversed Disc CAM Printed by A 3D FDM PLA and (F) Reversed Disc CAM Printed by A 3D FDM ABS+.

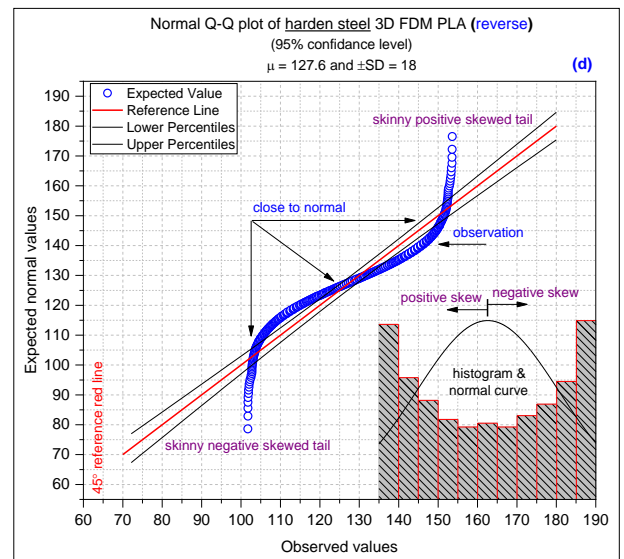
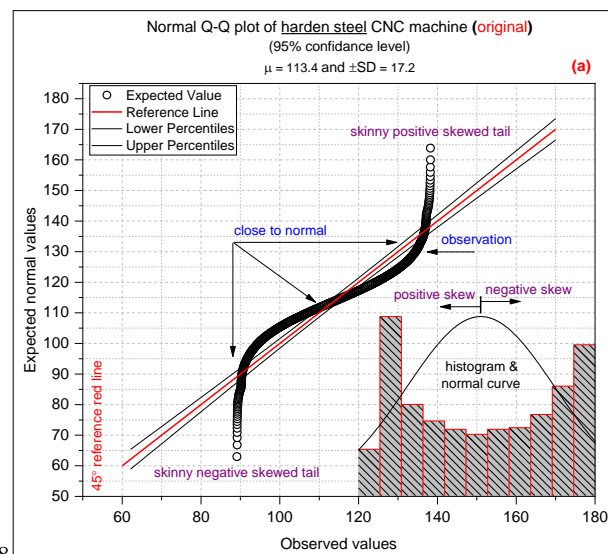
Figures 14, 15 and 16 show the obtained data from CMM used to plot the normal Q-Q plot (Quantile-Quantile plot) with a 95% level of confidence. Within the graphs, a histogram with a normal curve was plotted to show the frequency of the data obtained from the CMM machine for the existing part in the absence of original (existing) design data and reversed disc CAM. A 45-degree reference red line is also plotted. Figure 14 shows the normal Q-Q plot including the histogram for the original (existing) disc CAM of aluminum and reversed disc CAM including aluminum, hardened steel, stainless steel, PLA+, PLA, ABS+ and formlabs black V1 resin. Figure 15 shows the normal Q-Q plot including the histogram for the original (existing) disc CAM of hardened steel and reversed disc CAM including aluminum, hardened steel, stainless steel, PLA+, PLA, ABS+ and formlabs black V1 resin. Figure 16 shows the normal Q-Q plot including the histogram for the original (existing) disc CAM of stainless steel and reversed disc CAM including aluminum, hardened steel, stainless steel, PLA+, PLA, ABS+ and formlabs black V1 resin. The general trend for both original (existing) and reversed disc CAM showed equal distribution of expected normal values above and below the 45-degree reference line with the same pattern.

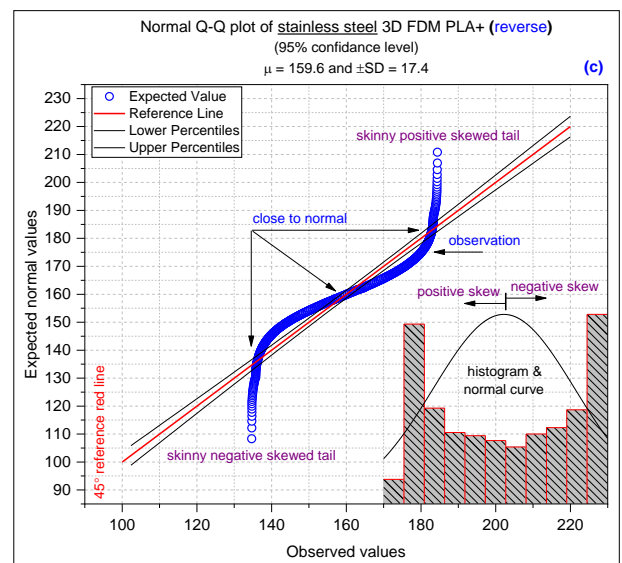
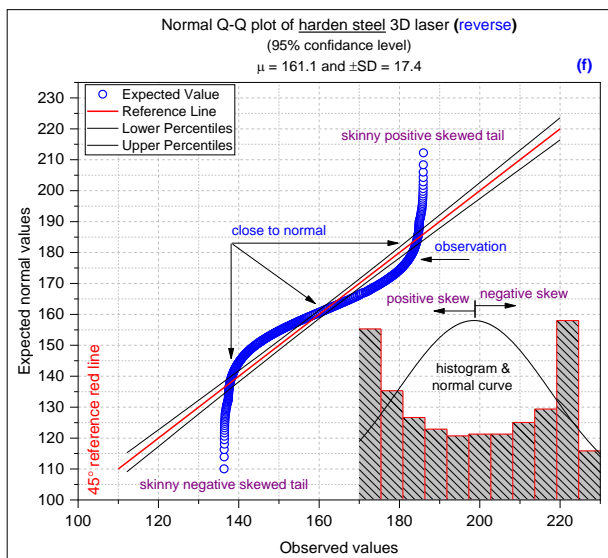
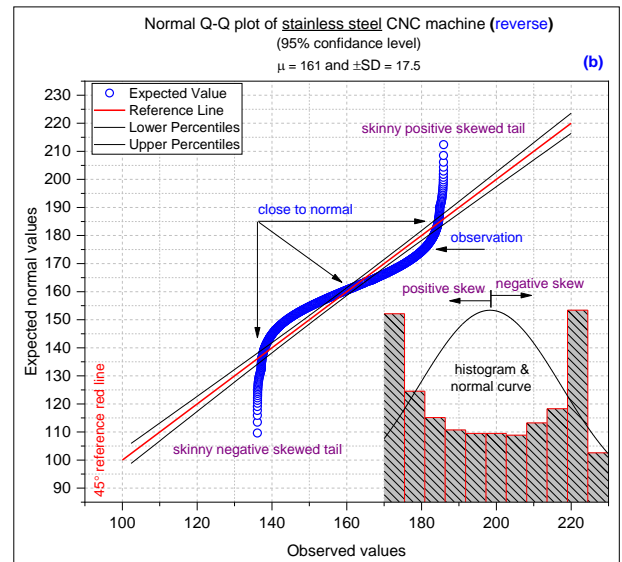
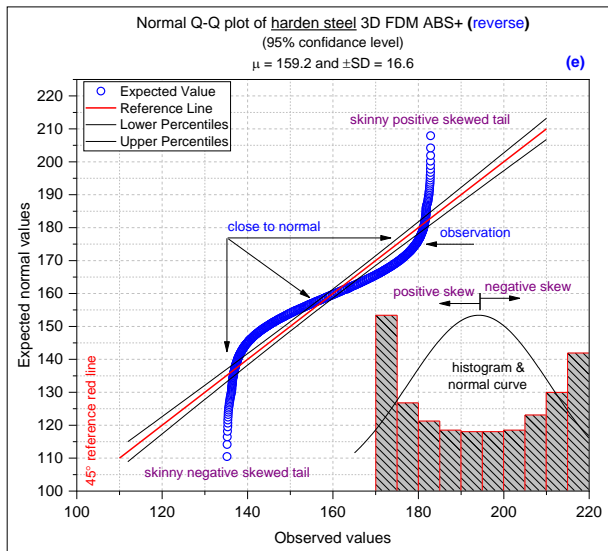
Generally, the blue circles in this Q-Q plot start out on one side of the line (skinny negative skewed tail) and then are almost entirely close to normal distribution and then move directly towards the other side of the reference line again (skinny positive skewed tail), indicating that this graph is a combination of two behaviours, starting at negatively skewed (showing an upward curve on the Q-Q plot) and ending at positively skewed (showing a downward curve on the Q-Q plot) with almost equally normal distribution. In these normal plots, the actual data points (observed values) are plotted on the x-axis and the expected normal values (Kaplan-Meier method) are plotted on the y-axis. Besides, as can be seen from Figures 14, 15 and 16, the standard deviation is approximately the same for all original (existing) and reversed disc CAMs, while the mean value varies from CAM to CAM, indicating that all procedures were precise but not necessarily accurate.



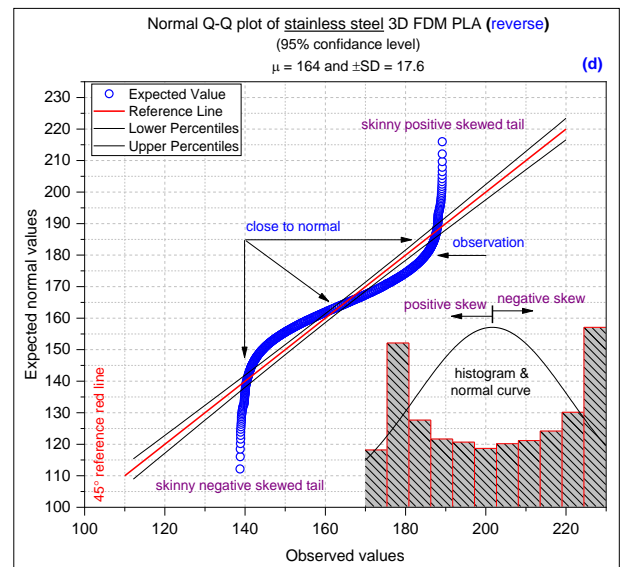
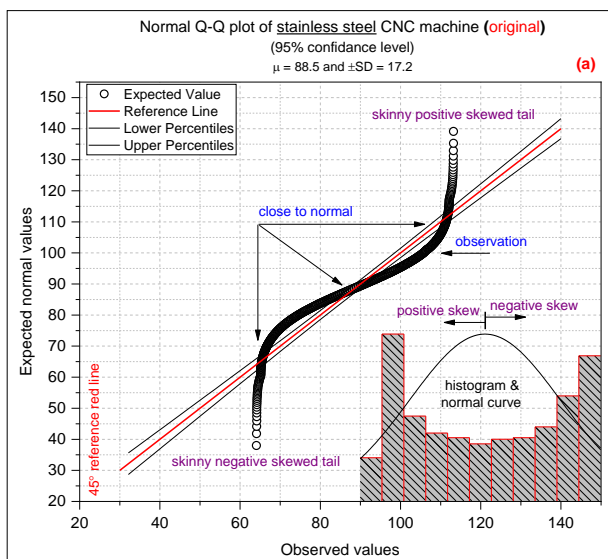


**Fig. 14:** Normal Q-Q Plot of Aluminium (A) Original Disc CAM Manufactured By CNC Machine and (B) Reversed Disc CAM Manufactured by CNC Machine (C) Reversed Disc CAM Printed by 3D FDM PLA+ (D) Reversed Disc CAM Printed by 3D FDM PLA (E) Reversed Disc CAM Printed by 3D FDM ABS+ and (F) Reversed Disc CAM Printed by 3D Laser.





**Fig. 15:** Normal Q-Q Plot of Hardened Steel (A) Original Disc CAM Manufactured by CNC Machine and (B) Reversed Disc CAM Manufactured by CNC Machine (C) Reversed Disc CAM Printed by 3D FDM PLA+ (D) Reversed Disc CAM Printed by 3D FDM PLA (E) Reversed Disc CAM Printed by 3D FDM ABS+ and (F) Reversed Disc CAM Printed by 3D Laser.



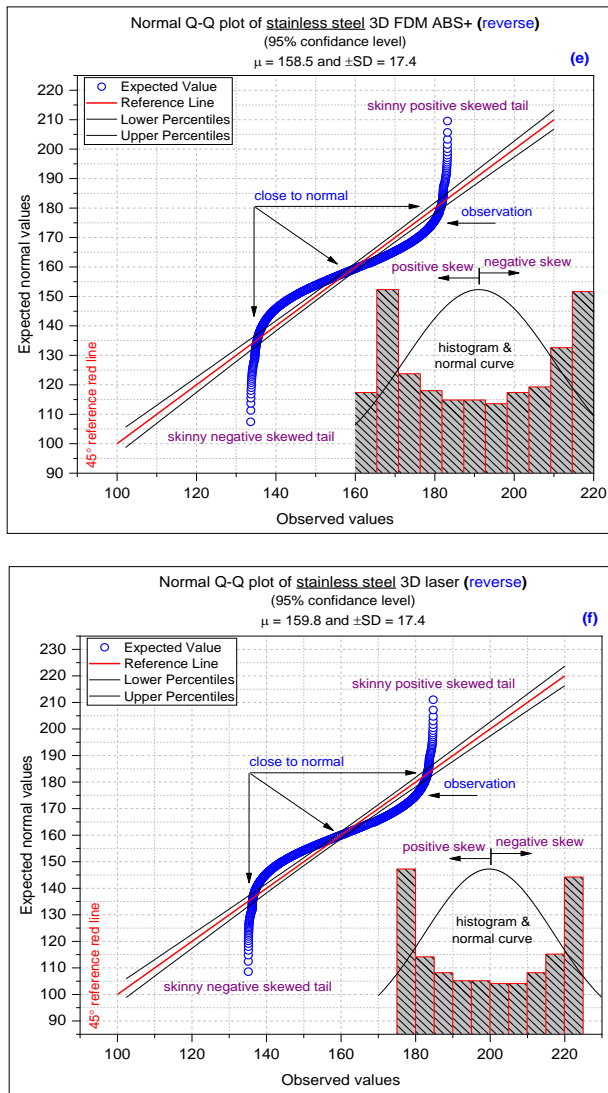


**Fig. 16:** Normal Q-Q Plot of Stainless Steel (A) Original Disc CAM Manufactured by CNC Machine and (B) Reversed Disc CAM Manufactured by CNC Machine (C) Reversed Disc CAM Printed by 3D FDM PLA+ (D) Reversed Disc CAM Printed by 3D FDM PLA (E) Reversed Disc CAM Printed by 3D FDM ABS+ and (F) Reversed Disc CAM Printed by 3D Laser.

## 4. Conclusions

Time taken to complete the design portion of the process can be reduced by using RE and RP techniques. RE is widely recognized as a useful cost-saving tool and is a systematic approach used to analyze the dimensions and design of an existing part so that one may derive potential improvements to the part or perform competitive benchmarking to understand the product further.

The analysis and the experimental considerations that have been made about the proposed disc CAM RE/CNC process and RE/RP process and led us to the following main conclusions and insights:

- The maximum value of the average height variation over the reversed disc CAM profile was 10.70 mm (for STL file of stainless steel) using 3D FDM PLA with a total increase in the height of almost ~7%.
- The minimum value of the average height variation over the reversed disc CAM profile was 9.55 mm (for an STL file of aluminum) using 3D FDM ABS+ with a total decrease in the height of almost ~5%.
- In the vertical axis (CG) and horizontal axis (AE), there are surpluses in the dimension of almost 4% to 6% from the original (existing) STL file of the disc CAM.

- In the diagonal axis (BF and DH), there is more deviation from the actual value of the original (existing) STL file of the disc CAM from almost 3% to 7%.
- The maximum value of the average surface roughness over the reversed disc CAM profile of the ABS+ material was 20.19  $\mu\text{m}$  (for an STL file of aluminum).
- The minimum value of the average surface roughness over the reversed disc CAM profile of the stainless steel was 0.64  $\mu\text{m}$  (for an STL file of stainless steel).
- The general trend of all reversed disc CAMs showed some positive skewness (+ve for steep peaks and flat valleys) and some negative skewness (-ve for flat peaks and steep valleys) with different degrees of equality.
- Q-Q plot with a 95% level of confidence showed that the standard deviation is approximately the same for all original (existing) and reversed disc CAMs, while the mean value varies from CAM to CAM, indicating that all procedures were precise but not necessarily accurate.

The results presented here show some significant increases in the height variation, geometric accuracy and surface roughness of the resulting reverse-engineered models compared to original (existing) disc CAM. Thus, the new material for a reversed disc CAM must be selected very carefully. These considerations reveal quite a few open issues and make clear the need to maintain investigation studies directed at developing new data processing software and cost-efficient RE/RP methodologies to give accurate answers to the precise requirements and the usability needs coming from the industrial demand for particular engineering materials for RE/RP and/or RE/CNC machine.

## Conflicts of Interest

The authors have no conflicts of interest.

## Funding Source

The authors received no financial support for the research and/or for the publication of this article.

## References

- [1] Raja, V. and K.J. Fernandes, Reverse Engineering - An Industrial Perspective. Springer Series in Advanced Manufacturing. 2018, UK, London: Springer-Verlag London.
- [2] Anwer, N. and L. Mathieu, from reverse engineering to shape engineering in mechanical design. CIRP Annals, 2016. 65(1): p. 165-168.
- [3] Lee, S.-J. and G.-J. Park, A novel method of reverse engineering using axiomatic design. Journal of Mechanical Science and Technology, 2014. 28(2): p. 595-604.
- [4] Rekoﬀ, M.G., on reverse engineering. IEEE Transactions on Systems, Man, and Cybernetics, 1985. SMC-15(2): p. 244-252.
- [5] Motavalli, S., Object-oriented modelling of a feature-based reverse engineering system. International Journal of Computer Integrated Manufacturing, 1996. 9(5): p. 354-368.
- [6] Chikofsky, E.J. and J.H. Cross, Reverse engineering and design recovery: a taxonomy. IEEE Software, 1990. 7(1): p. 13-17.
- [7] Otto, K.N. and K.L. Wood, Product Evolution: A Reverse Engineering and Redesign Methodology. Research in Engineering Design, 1998. 10(4): p. 226-243.
- [8] Ullman, D., the Mechanical Design Process. 4th Edition ed. McGraw-hill Series in Mechanical Engineering. 2009, Dubuque, IA McGraw-Hill: McGraw-Hill Education.
- [9] Huang, S.H., et al., Additive manufacturing and its societal impact: a literature review. The International Journal of Advanced Manufacturing Technology, 2013. 67(5): p. 1191-1203.
- [10] Majstorovic, V., et al., Reverse engineering of human bones by using method of anatomical features. CIRP Annals, 2013. 62(1): p. 167-170.
- [11] Erdős, G., T. Nakano, and J. Váncza, Adapting CAD models of complex engineering objects to measured point cloud data. CIRP Annals, 2014. 63(1): p. 157-160.

- [12] Laroche, F., A. Bernard, and B. Hervy, DHRM: A new model for PLM dedicated to product design heritage. *CIRP Annals*, 2015. 64(1): p. 161-164.
- [13] Várady, T., R.R. Martin, and J. Cox, Reverse engineering of geometric models—an introduction. *Computer-Aided Design*, 1997. 29(4): p. 255-268.
- [14] Xia, Z., Application of Reverse Engineering based on Computer in Product Design. *International Journal of Multimedia and Ubiquitous Engineering*, 2014. 9(5): p. 343-354.
- [15] Mostafa, M.A.G., M.S. Alsoufi, and B.A. Tayeb, CAD/CAM Integration Based on Machining Features for Prismatic Parts. *International Journal of Emerging Trends & Technology in Computer Science* 2015. 4(3): p. 106-110.
- [16] Alsoufi, M.S. and A.E. Elsayed, Warping Deformation of Desktop 3D Printed Parts Manufactured by Open Source Fused Deposition Modeling (FDM) System. *International Journal of Mechanical and Mechatronics engineering*, 2017. 17(4): p. 7-16.
- [17] Alsoufi, M.S. and A.E. Elsayed, How Surface Roughness Performance of Printed Parts Manufactured by Desktop FDM 3D Printer with PLA+ is influenced by Measuring Direction. *American Journal of Mechanical Engineering*, 2017. 5(5): p. 211-222.
- [18] Alsoufi, M.S. and A.E. Elsayed, Surface Roughness Quality and Dimensional Accuracy - A Comprehensive Analysis of 100% Infill Printed Parts Fabricated by a Personal/Desktop Cost-Effective FDM 3D Printer Materials Sciences and Applications, 2018. 9(1): p. 11-40.
- [19] Alsoufi, M.S. and A.E. Elsayed, Quantitative analysis of 0% infill density surface profile of printed part fabricated by personal FDM 3D printer *International Journal of Engineering & Technology*, 2018. 7(1): p. 44-52.
- [20] Alsoufi, M.S., et al., Experimental Characterization of the Influence of Nozzle Temperature in FDM 3D Printed Pure PLA and Advanced PLA+. *American Journal of Mechanical Engineering*, 2019. 7(2): p. 45-60.
- [21] Alsoufi, M.S. and T.M. Bawazeer, Quantifying assessment of touch-feel perception: an investigation using stylus base equipment and self-touch (human fingertip). *Umm Al-Qura University: Journal of Engineering and Architecture*, 2015. 1(1): p. 1-16.
- [22] Alsoufi, M.S. and T.M. Bawazeer, The Effect of Aggressive Biological Materials on a Painted Automotive Body Surface Roughness. *American Journal of Nano Research and Applications*, 2015. 3(2): p. 17-26.
- [23] Suker, D.K., et al., Studying the Effect of Cutting Conditions in Turning Process on Surface Roughness for Different Materials. *World Journal of Research and Review (WJRR)* 2016 2(4): p. 16-21.
- [24] Alsoufi, M.S., et al., Experimental Study of Surface Roughness and Micro-Hardness Obtained by Cutting Carbon Steel with Abrasive WaterJet and Laser Beam Technologies. *American Journal of Mechanical Engineering*, 2016. 4(5): p. 173-181.
- [25] Bawazeer, T.M., et al., Effect of Aqueous Extracts of *Salvadora Persica* "Miswak" on the Acid Eroded Enamel Surface at Nano-Mechanical Scale. *Materials Sciences and Applications*, 2016. 7(11): p. 754-771.
- [26] Alsoufi, M.S., et al., Surface Roughness and Knoop Indentation Micro-Hardness Behavior of Aluminium Oxide ( $Al_2O_3$ ) and Polystyrene ( $C_8H_8$ )<sub>n</sub> Materials *International Journal of Mechanical & Mechatronics Engineering* 2016. 16(6): p. 43-49.
- [27] Alsoufi, M.S., State-of-the-Art in Abrasive Water Jet Cutting Technology and the Promise for Micro- and Nano-Machining. *International Journal of Mechanical Engineering and Applications*, 2017. 5(1): p. 1-14.
- [28] Alsoufi, M.S., et al., Influence of Abrasive Waterjet Machining Parameters on the Surface Texture Quality of Carrara Marble. *Journal of Surface Engineered Materials and Advanced Technology*, 2017. 7(2): p. 25-37.
- [29] Alsoufi, M.S., et al., Abrasive WaterJet Machining of Thick Carrara Marble: Cutting Performance vs. Profile, Lagging and WaterJet Angle Assessments. *Materials Sciences and Applications*, 2017. 8(5).
- [30] Alsoufi, M.S., et al., The Effect of Detergents on the Appearance of Automotive Clearcoat Systems Studied in an Outdoor Weathering Test *Materials Sciences and Applications*, 2017. 8(7): p. 521-536.
- [31] Dong, W.P., P.J. Sullivan, and K.J. Stout, Comprehensive study of parameters for characterizing three-dimensional surface topography I: Some inherent properties of parameter variation. *Wear*, 1992. 159(2): p. 161-171.
- [32] Dong, W.P., P.J. Sullivan, and K.J. Stout, Comprehensive study of parameters for characterizing three-dimensional surface topography II: Statistical properties of parameter variation. *Wear*, 1993. 167(1): p. 9-21.
- [33] Dong, W.P., P.J. Sullivan, and K.J. Stout, Comprehensive study of parameters for characterizing three-dimensional surface topography III: parameters for characterising amplitude and some functional properties. *Wear*, 1994. 178(1): p. 29-43.
- [34] Dong, W.P., P.J. Sullivan, and K.J. Stout, Comprehensive study of parameters for characterising three-dimensional surface topography: IV: Parameters for characterising spatial and hybrid properties. *Wear*, 1994. 178(1-2): p. 45-60.
- [35] Thomas, T.R., Characterization of surface roughness. *Precision Engineering*, 1981. 3(2): p. 97-104.
- [36] Edwart, C., *Technika komputerowa CAx w inzynierii produkcji* (Polish). 2000, polski: Wydawnictwo WNT.
- [37] Alsoufi, M.S., A high dynamic response micro-tribometer measuring-head, in *School of Engineering*. 2011, University of Warwick: Coventry.
- [38] Alsoufi, M.S., Dry Micro-frictional Properties of Ceramic and Polystyrene Oscillating Against a Sapphire Counterbody at Small-Scale Loads. *Engineering and Technology*, 2016. 3(5): p. 100-105.
- [39] Chetwynd, D.G. and M.S. Alsoufi. A novel micro-friction measuring-head using force-feedback compensation. in *Proc. SPIE 7544, Sixth International Symposium on Precision Engineering Measurements and Instrumentation*. 2010. Hangzhou, China.